scientific reports

Check for updates

OPEN

In vitro release kinetics of bioactive compounds (gallic acid, ellagic acid, and eugenol) from chitosan polymer and the bioactivity of herb-loaded chitosan–CuO nanocomposites

Geethma Ekanayake, Supuni Wijayawardana, Madara Jayanetti, Charitha Thambiliyagodage✉, Heshan Liyanaarachchi & Amavin Mendis

The biological efficacy of nanocomposites comprised of chitosan, CuO nanoparticles, and extracts of *Phyllanthus emblica*, and *Syzygium aromaticum* was studied. The study assessed the pH– and ionic strength-responsive controlled release of the bioactive compounds, gallic acid, ellagic acid and eugenol, from the chitosan biopolymer. Release data were fitted into zero-order, first-order, Korsmeyer–Peppas (KP), Peppas–Sahlin (PS), Higuchi, and Hixson–Crowell kinetic models to evaluate the release mechanism. According to KP and PS models ($R^2 \geq 0.96$), release was governed by quasi-Fickian diffusion ($n < 0.43$), where the diffusion occurs along with the polymer relaxation and swelling. *P.emblica*-coated chitosan (*PeC*) composite exhibited a burst release at acidic media conditions, and a quasi-Fickian diffusion at pH 5.5–7.4. Higher ionic strength caused salting-in effects for *PeC* in 0.4 M media, resulting in a transiently increased release. In acidic conditions, diffusion-controlled release was observed for *S.aromaticum*-coated chitosan (*SaC*) composite, with the optimal release at pH 4 media. Release was facilitated by hydrophobic nanochannels at elevated pH (8.5–10) and ionic strength of 0.5 M NaCl. The PS model's relaxation contributions were significant at 0.4 M NaCl and 5 mg drug loading. Both composites demonstrated enhanced release at physiological conditions (0.1–0.2 M NaCl, pH 7.4). Sustained release of *SaC* was achieved in near-neutral/moderate ionic strength media, whereas *PeC* exhibited sustained release in acid/low ionic strength media. The *PeC* and *SaC* composites showed IC_{50} values of 10.78 µg/mL and 19.27 µg/mL for the DPPH radical scavenging ability, respectively. Recorded IC_{50} values for the egg albumin denaturation assay were 467 µg/mL and 390.44 µg/mL, respectively. The antibacterial activity against *Escherichia coli*, *Pseudomonas aeruginosa*, *Klebsiella pneumoniae*, and *Staphylococcus aureus* showed maximum inhibition zones of 11.83 ± 0.06 mm (Chitosan: CuO 1:2), 12.67 ± 0.20 mm (1:4), 16.50 ± 0.09 mm (1:4), and 11.83 ± 0.08 mm (4:1), respectively. Among the herbal-coated samples, *SaC* exhibited the highest activity of 23.67 ± 2.84 mm against *E. coli*.

Keywords Drug delivery, Chitosan, Eugenol, Gallic acid, Ellagic acid

The range of dosages that maximize therapeutic effectiveness while avoiding undesirable side effects or toxicity is known as a therapeutic window or safety window. Maintaining the dosage within this range guarantees both efficacy and safety[1]. Although plant derived phytochemicals possess beneficial pharmacological properties, they have limited bioavailability due to poor solubility and stability[2]. Toxicity is also another concern related to the pharmaceutical constituents, specifically when the higher dosages are used to overcome issues related to bioavailability[3]. Chemical modifications, encapsulation and the use of delivery systems are employed to reduce toxicity while enhancing bioavailability, stability, and dispersibility. *Phyllanthus emblica*, commonly known

Department of Applied Sciences, Faculty of Humanities and Sciences, Sri Lanka Institute of Information Technology, Malabe, Sri Lanka. ✉email: charitha.t@sliit.lk

as Alma or Indian gooseberry, is a deciduous tree of the family Phyllanthaceae[4]. *Phyllanthus emblica* has a variety of medicinal qualities, such as anti-inflammatory, anti-oxidant [4,5], anti-cancer[6,7], immunomodulatory[8], cytoprotective[9], anti-viral[10], anti-jaundice[11], anti-dyslipidemic[12], anti-ageing[13], hepatoprotective[14], nephroprotective[15], and anti-diabetic[16] effects. The main phenolic components of *P. emblica* fruits are hydrolyzable tannins, which account for 35% of the powdered dried fruit and 4% of the fresh fruit weight. The two primary categories of hydrolyzable tannins, known as gallotannins (esters of gallic acid) and ellagitannins (esters of ellagic acid), are extensively distributed in many plant families. The bioavailability of ellagitannins and ellagic acid in *P. emblica* has not been extensively studied. However, research on other sources of these compounds, including Punicacea[17] and Rosaceae[18], suggest poor bioavailability has resulted due to the lower absorption in the small intestines and breakdown into less potent antioxidant forms[19].

Syzygium aromaticum, commonly known as clove, is a dried flower bud belonging to the family Myrtaceae[20]. Clove is excessively used as a pharmacological substance for its antibacterial[21], antiviral[22], anti-inflammatory[20], antioxidant[23], anti-carcinogenic[24], anti-thrombotic[25] and anti-parasitic[26] activities. Clove buds have 15–20% essential oil, mainly composed of eugenol (70–85%), eugenyl acetate (15%) and β-caryophyllene (5–12%)[27]. Eugenol can, however, result in systemic toxicity at higher dosages, which can harm the liver and produce additional adverse reactions[28]. Eugenol has low oral bioavailability (4%), even after administering 20 mg/kg of eugenol intravenously for rat models[29]. Therefore, to address the dual challenges of toxicity and bioavailability, it is proposed that intestinal absorption be reduced by designing targeted drug delivery systems with sustained release to maintain therapeutic doses over time without reaching harmful peak concentrations.

With its antibacterial[30], catalytic[31], anti-carcinogenic[32], and biosensing properties[33], copper oxide (CuO) nanoparticles (NPs) are versatile and affordable materials with important biomedical applications. CuO NPs have special physicochemical qualities, including occurrence in various oxidation states and thermal stability and chemical inactivity due to the lower band gap energy (~2 eV)[34]. Because of their potent antibacterial activities, which are effective against a wide range of gram-positive and negative bacteria[34], CuO NPs are used in nosocomial infections and wound dressings[35]. Studies have shown CuO NPs can be coated with plant extracts, improving the inherent antimicrobial activity[36]. Nevertheless, toxicity issues restrict their application since CuO NPs can produce reactive oxygen species (ROS), which can harm cells (specifically mammalian cells) and DNA[37]. Thus, it is essential to guarantee biocompatibility and non-toxicity for their safe use in clinical and diagnostic contexts.

Drug delivery systems facilitate the sustained release of the drug over a prolonged period, preventing its premature degradation before it reaches the targeted site[38]. A variety of approaches have been used in the construction of drug delivery systems in recent studies, including liposomes[39], nanoemulsions[40], drug-coated nanoparticles[41] and polymer-based approaches[42,43]. Among the delivery systems, bio-polymeric nanoparticles have received the greatest attention because of their superior biocompatibility, capacity to store hydrophilic or hydrophobic drugs, significant stability, and potential for administration via many routes[38]. For instance, Gaur et al.[44] used PLGA and chitosan for protein-based drugs; Yadav et al.[45] used a metal–organic framework (MIL-100(Fe)) for Norfloxacin; Zhang et al.[46] developed a multilayer system (chitosan, hyaluronic acid, Eudragit S100) for dexamethasone; and Mohammadi et al[47] used a nanocomposite hydrogel (carboxymethylcellulose, polyacrylic acid, starch-modified Fe_3O_4) for anticancer drugs (doxorubicin, 5-FU).

Chitosan, a derivative of chitin via n-deacetylation, is a desirable candidate due to its availability, ease of extraction, non-toxic nature, biocompatibility and biodegradability[48]. Intrinsic properties of chitosan, such as its bacteriostatic nature and anti-inflammatory activity, add further to the value of the biopolymer in medical applications[49]. In recent years, chitosan has been widely explored in creating drug delivery systems alone or in combination with other polymers. Studies by Adimmolam et al. reported the delivery of doxorubicin by chitosan stabilized magnetite nanoparticles[50]. Pulmonary delivery of Baclofen was achieved by Ni et al.[51] using functionalized trimethyl chitosan system, and Nair[52] has delivered lipophilic curcumin using chitosan nanoparticles. Chitosan can also be used as a stabilizing, capping and chelating agent in the CuO NPs synthesis, which prevents the aggregation of the NPs and controls the shape and uniformity of synthesized NPs by regulating the bioavailability of ions during the synthesis process. Several studies have reported the use of chitosan as a capping and stabilizing agent in the CuO NPs synthesis[53,54], and the enhanced antibacterial and anticancer activity of the nanocomposites composed of chitosan and CuO NPs was also reported in the literature[55,56]. Therefore, it is evident that the incorporation of chitosan into the CuO NPs can enhance the biological activity, specifically the antibacterial potential, of the nanocomposites. However, no studies were reported to test the antimicrobial activity of the chitosan/CuO nanocomposites in different ratios against a vast range of microbes.

In the current study, chitosan was used as a chelating agent during the hydrothermal treatment process of synthesizing the Chitosan: CuO (Chi: CuO) nanocomposites in different ratios. Even though chitosan has been utilized to deliver natural bioactive compounds like curcumin[57,58], ellagic acid[59], quercetin[60], chlorogenic acid[61] and gallic acid[62], to our knowledge the *P. emblica* extract and *S. aromaticum* extract coated chitosan biopolymers have not been studied for the effective release of bioactive compounds (gallic acid, ellagic acid and eugenol) using drug release kinetic models. In the current study, the drug release kinetics were studied using six kinetic models and the biological efficacy of the drug composite was evaluated. Further, antimicrobial activity of the synthesized CuO NPs, chitosan, Chi: CuO nanocomposites and plant extract coated composites were tested against test organisms *Staphylococcus aureus*, *Escherichia coli*, *Klebsiella pneumoniae* and *Pseudomonas aeruginosa*.

Materials and methodology

Chemicals and materials

Penaeus vannamei (shrimp) shells were sourced from Ceylon Catch (Pvt) Ltd., HCl (37%), methanol, and HNO_3 (68%) were procured from Sigma Aldrich (Gillingham SP8 4XT, United Kingdom), NaOH pellets, $CuSO_4$, Dimethyl sulfoxide (DMSO), and Folin–Ciocâlteu reagent (2N) were purchased from Sisco Research

Laboratories (Pvt) Ltd. (Mumbai, India), the herbs *Phyllanthus emblica* fruits, and *Syzygium aromaticum* dried flower buds were purchased from a local market in Kandy, Sri Lanka. Muller Hinton Agar (MHA) and Luria Bertani Broth (LB broth), DPPH (2,2-Diphenyl-1-picrylhydrazyl) were purchased from HiMedia Laboratories (Germany), Deionized water (DI), with resistivity greater than 18.0 MΩ.cm (Millipore Milli-Q system), was used in the experiments. All of the chemicals utilized in the experiments were of analytical grade and were used without further purification.

Bacterial pathogens used for the study, the test organisms, gram-negative *Escherichia coli*, *Pseudomonas aeruginosa*, *Klebsiella pneumoniae*, and gram-positive *Staphylococcus aureus*, were procured from the Medical Research Institute, Sri Lanka.

Synthesis of chitosan from shrimp shells

The sourced shrimp shells were washed several times with deionized water followed by two rounds of washing with isopropyl alcohol to remove impurities. The washed shells were then dried in an oven at 60 °C and crushed using a grinder until a fine powder consistency was achieved. Demineralization (removal of $CaCO_3$ and $Ca_3(PO_4)_2$) of shrimp shell powder was carried out next, by suspending the powder in a 10% (v/v) HCl solution for 24 h. Then, the acid was washed off with deionized water until a neutral pH was achieved. The resultant wet powder was then left in a 3% NaOH solution for 5 h while stirring to remove the proteins. Deacetylation was done next by refluxing the powder in 50% NaOH for 2 h at 80 °C, where chitin from the shells was converted to chitosan. After that, the powder was thoroughly washed with deionized water to remove the base, and a neutral pH was obtained. The resulting chitosan was then hydrothermally treated at 150 °C for 15 h, dried in an oven, and stored in an airtight container for further use and analysis.

Synthesis of CuO nanoparticles

The required weight of the $CuSO_4$ powder to yield the desired CuO mass in chitosan: CuO ratios of 1:1, 1:2, 1:3, 1:4, 2:1, 3:1, and 4:1 was calculated based on the stoichiometric conversion. The weighed $CuSO_4$ powder was dissolved in a minimum amount of deionized water until a completely dissolved solution was obtained. 1% NaOH solution was added to the mixture dropwise and stirred for two hours until a dark blue precipitate appeared. Then, stirring was continued overnight until a black precipitate was obtained.

Synthesis of the nanomaterial

Samples were synthesized in different weight ratios of chitosan:CuO as follows; Chitosan:CuO 1:1, 1:2, 1:3, 1:4, 2:1, 3:1, 4:1. These are abbreviated in the text, as (Chi:CuO 1:1), (Chi:CuO 1:2), (Chi:CuO 1:3), (Chi:CuO 1:4), (Chi:CuO 2:1), (Chi:CuO 3:1), and (Chi:CuO 4:1) respectively. Required weights of both chitosan and CuO to obtain the above-mentioned ratios were measured. The two were mixed with the necessary amount of water and sonicated for 2 h to homogenize the solution. Then the mixture was hydrothermally treated at 150°C for 15 h to obtain the nanocomposites. Then the obtained samples were filtered and washed with deionized water until the samples were free of Cl^- and SO_4^{2-} ions, and a neutral pH was achieved. The washed samples were then oven-dried at 100 °C until completely dried and stored for further analysis.

Preparation of herbal extracts

Phyllanthus emblica fruits and *Syzygium aromaticum* dried flower buds were cleaned using deionized water, cut into small pieces, and oven-dried at 40 °C overnight until the moisture completely evaporated and fully dried. The dried herbs were then ground to a fine powder. The powders were dissolved in methanol and were shaken in a rotary shaker for two days followed by ultrasonication for two hours at °C. The sonicated mixture was then centrifuged for 3 min at 3000 rpm. Then the methanolic extract was taken and the pellet was discarded. The extract was then evaporated at 40 °C to get rid of the solvent and the extract concentrate was obtained.

Fabrication of loaded nanocomposites

Hydrothermally treated chitosan, CuO nanoparticles, and two chitosan/CuO nanocomposites (corresponding to the formulations with the highest chitosan and highest CuO content, respectively) were loaded with *Phyllanthus emblica* and *Syzygium aromaticum* methanolic extracts to obtain herb-loaded nanocomposites. The nanomaterials were dispersed in the plant extracts and subjected to slow solvent evaporation under continuous stirring to promote uniform surface coating. The coated nanocomposites were subsequently dried at 40 °C to eliminate residual moisture and were stored in desiccated, light-protected, airtight containers until further analysis.

Phytochemical analysis

The presence of several phytoconstituents including carbohydrates (Fehling's, Benedict's, iodine tests), proteins (ninhydrin), alkaloids, glycosides (Salkowski's, Keller-Kilani's tests), terpenes, steroids, flavonoids (alkaline reagent test), phenols and tannins, saponins, alkaloids was assessed in the in *Phyllanthus emblica*, and *Syzygium aromaticum* plant crude extracts in methanol. The analysis was conducted through a series of well-established precipitation and coloration reactions, as documented in standard reference literature. Methanol and aqueous media were employed as solvents for the tests[63,64].

Material characterization

X-ray diffraction (XRD) patterns were acquired using a D8 Advance Bruker diffractometer equipped with Cu Kα radiation (λ = 0.154 nm). The diffraction angle (2θ) was scanned from 5 to 80° at a rate of 2°/min. The morphology of the synthesized nanocomposites was examined using transmission electron microscopy (TEM) on a JEOL JEM 2100 instrument operated at an accelerating voltage of 200 kV. Prior to TEM analysis, a 1 µL aliquot of the

sample was deposited onto a carbon-coated copper grid with holes and allowed to dry at room temperature. Scanning electron microscopy (SEM) images were obtained using a ZEISS EVO 18 RESEARCH instrument. Surface chemical composition and oxidation states were analyzed using X-ray photoelectron spectroscopy (XPS) on a Thermo Scientific ESCALAB Xi + spectrometer, which provided both survey spectra and high-resolution spectra of the synthesized catalysts. Optical properties were evaluated using a Shimadzu 1800 UV–visible spectrophotometer, which features a high-precision Czerny-Turner optical system. Raman spectroscopy was performed using a Bruker Senterra Raman microscope spectrophotometer to further characterize the structural properties of the samples.

Antioxidant assay

The antioxidant potential of *Phyllanthus emblica, Syzygium aromaticum* plant crude extracts, and herb-loaded chitosan was evaluated using a stable 1,1-diphenyl-2-picrylhydrazyl (DPPH) radical scavenging assay. To the prepared concentration series (5, 10, 15, 20, 25 µg/mL) of the extracts, 0.5 mL of the 1 mM DPPH stock solution was added, and the absorbance was measured against the blank solution at 517 nm after 30-min incubation in the dark. All experiments were performed in triplicate (n = 3), and the results were expressed as mean % inhibition of the DPPH radical (RSA%) ± standard error (SE), calculated using the following formula:

$$Radical Scavenging Activity(\ \mathrm{RSA}\%) = \frac{Abs of control - Abs of sample}{Abs of control} \times 100 \quad (1)$$

The IC_{50} value, representing the concentration of the sample required to scavenge 50% of the DPPH radicals, was determined by plotting RSA% against concentration using a linear regression model.

Anti-inflammatory assay

The in vitro anti-inflammatory activity of *Phyllanthus emblica, Syzygium aromaticum* plant crude extracts, and herb-loaded chitosan was evaluated using an egg albumin denaturation assay. The prepared concentration series (100–700 µg/mL) of the test samples was added to the reaction mixture (5 mL) consisting of 0.2 mL of 1% (w/v) egg albumin, 2.8 mL of phosphate-buffered saline (PBS, pH 6.4). Absorbance was measured at 660 nm after incubation at 37 °C for 30 min, followed by heating in a water bath at 70 °C for 15 min. Diclofenac sodium was used as the positive control, and the experiment was triplicated. The percentage inhibition of protein denaturation was calculated using the following formula:

$$\%\ \text{Inhibition of egg albumin denaturation} = \frac{Abs of sample - Abs of control}{Abs of control} \times 100 \quad (2)$$

The IC_{50} value, representing the concentration of the extract required to inhibit 50% of egg albumin denaturation, was determined through linear regression analysis. Results were reported as mean % inhibition ± standard error.

Total phenolic content

To quantify the total phenolic content of *Phyllanthus emblica*, *Syzygium aromaticum* plant crude extracts, and herb-loaded chitosan, 0.5 mL of the sample solution was mixed with 0.1 mL of Folin-Ciocalteu reagent (0.5 N) and incubated at room temperature in the dark for 15 min. Subsequently, 2.5 mL of 7.5% sodium carbonate solution was added to the mixture, which was then incubated for an additional 2 h in the dark at room temperature. The absorbance of the resulting solution was measured at 760 nm using a UV/VIS spectrophotometer. The total phenolic content was expressed as milligrams of gallic acid equivalent per gram of dry extract (mg GAE/g). A standard curve was constructed using gallic acid, with a linear calibration range of 10 to 70 µg/mL.

Drug release study

The in vitro drug release profile of the synthesized herb-loaded chitosan composite with both *Phyllanthus emblica* and *Syzygium aromaticum* was evaluated under varying pH conditions (pH 1, 2.5, 4, 5.5, 7, 7.4, 8.5, and 10) and ionic strengths, adjusted by altering NaCl concentrations (0.1–0.5 M). For the analysis, 5 mg of the composite material was dispersed in the release medium within a plastic cuvette. Drug release data were collected at 15-min intervals over a 10-h period using a visible range spectrophotometer. Based on the absorbance values, the optimal pH and NaCl concentration for maximum drug release were identified. To assess dose-dependent release, a medium containing 0.2 M NaCl at pH 7.4 was prepared. Drug release was measured in this medium using varying composite weights (2.5, 5, 7.5, and 10 mg). The cumulative drug release percentage (CDR%) was calculated using the following equation:

$$\mathrm{CDR}\% = \frac{Absorbance\ value\ at\ time\ t_1}{Total\ amount\ of\ drug\ encapsulated\ with\ delivery\ system} \times 100 \quad (3)$$

The total amount of drug encapsulated in the chitosan biopolymer was estimated based on the plant powder-to-biopolymer ratio.

Statistical analysis

All experiments were conducted in triplicate, and results were expressed as mean ± standard error (SE). Statistical significance ($p < 0.05$) between treatment means was determined using one-way analysis of variance (ANOVA) performed with SPSS 27 (SPSS Inc., Chicago, Illinois, USA).

Drug release kinetic models

To elucidate the release mechanisms of *Phyllanthus emblica*, and *Syzygium aromaticum* extracts from the chitosan biopolymer, the obtained release data under varying pH, ionic strength, and drug concentrations were fitted to six kinetic models: zero-order, first-order, Korsmeyer – Peppas, Peppas–Sahlin, Higuchi, and Hixson–Crowell models. The corresponding model equations are stated below in Table 1.

Antibacterial activity

Microbial strain and inoculum preparation

For preparing the inoculum, *Escherichia coli, Staphylococcus aureus, Pseudomonas aeruginosa,* and *Klebsiella pneumoniae* were cultured in Luria Bertani broth medium at 37 °C overnight. The microbial cultures were sub-cultured and overgrown 24 h prior to the assay and later diluted and adjusted concentrations to obtain a microbial suspension of 5×10^5 colony-forming units (CFUs)/mL using the spectrophotometer for further analysis.

Agar well diffusion method

Nanomaterials, nanocomposites, and plant extracts were weighed (20, 40, and 60 mg), and sonicated to disperse in Dimethyl sulfoxide (DMSO) for 1 h. The Mueller Hinton Agar plate surface was inoculated by spreading the adjusted microbial inoculum of 5×10^5 colony-forming units (CFUs)/ml over the entire agar surface via streaking. Holes were punched aseptically with a sterile cork borer and a volume (70 µL) of the antimicrobial agent solution of desired concentrations; 20, 40, and 60 mg in 1 mL of DMSO was introduced into the wells. Amoxicillin which is a standard antibiotic and Dimethyl sulfoxide (DMSO) were used as positive and negative control, respectively. Then the agar plates were incubated at 37 °C for about 18 h and the zones of inhibition were measured in mm with the use of a metric ruler from the back of the Petri plate. Three replicates were prepared for each sample and each bacterial species. Results were reported as mean ± standard error (n = 3).

Minimum inhibitory (MIC), and minimum bactericidal (MBC) concentration evaluation

The antibacterial agents prepared were diluted to obtain a concentration series, 0.3125, 0.625, 1.25, 2.5, 5, 10, 20, and 40 mg/ml, and a control in sterile Eppendorf tubes. MIC was determined by inoculating 1 mL of each microbial culture (0.5 McFarland standard) to a test tube containing 2 mL of antibacterial agent in Luria Bertani broth. MBCs were determined by plating onto nutrient agar plates. In detail, 2 µL of the treated samples containing the nanomaterial and the test organism from each test tube, were inoculated into Muller Hinton agar plates for the determination of MBC. Both the test tubes and the plates were then incubated at 37 °C for 18 to 24 h and thereafter observed for the growth of bacteria and viable count, respectively.

The minimum incubation concentration (MIC) of nanocomposite suspension was determined as the concentration at which there was no visible turbidity. In contrast, MBC was determined as the lowest concentration of nanocomposite suspension that prevented the growth of bacteria yielding three log reductions (99.9%) on spread plates.

Time-kill synergy assay

To determine the antibacterial activity of the synthesized nanomaterials against the test bacterial pathogens, 2 mL of the each bacterial culture and 1 mL of the each nanosuspensions prepared were mixed. The time-kill synergy assay was carried out by broth macro dilution method while the samples were kept in a rotary shaker at 200 rpm. The optical density was measured at intervals of 1 h for a total of 12 h using 600 nm wavelength. Turbidity was shown on a graph against time. To investigate for any indications of antibacterial actions of the synthesized nanocomposite, the growth curve thus obtained was examined. The positive control utilized was amoxicillin. The negative control was DMSO; the solvent used to dissolve the sample.

High-performance liquid chromatography (HPLC) analysis

The HPLC fingerprint of the methanolic *Phyllanthus emblica* extract was performed using an Aglient 1200 HPLC system equipped with ZORBAX RRHT Eclipse XDB-C18 column (5 µm × 4.6 mm × 150 mm). Detection was carried out at 254 nm using a UV–Vis detector. The mobile phase consisted of (A) 0.1% orthophosphoric acid in water: methanol (95:5, v/v) and (B) acetonitrile:0.5% acetic acid in water. Gradient elution was employed as follows: 0–5 min, 0% B; 5–20 min, 0–15% B; 20–30 min, 15–25% B; 30–35 min, 25–30% B; 35–36 min, 35–0%

Model	Model equation
Zero-order	$Q_t = Q_0 + k_0 t$ (4)
First-order	$Q_t = Q_0(1 - e^{-k_1 t})$ (5)
Korsmeyer – Peppas	$Q_t = k_P t^n$ (6)
Peppas–Sahlin	$Q_t = k_D t^m + K_R t^{2m}$ (7), $\frac{R}{F} = \frac{K_R t^m}{K_D}$ (8)
Higuchi	$Q_t = k_H t^{1/2}$ (9)
Hixson–Crowell	$Q_0^{1/3} - Q_t^{1/3} = k_{HC} t$ (10)

Table 1. Mathematical equations of each model used to fit the drug release kinetics.

B; 36–45 min, isocratic elution with 0% B. The total running time was 45 min, and the column temperature was maintained at 30°C. The injection volume was 10.0 µL.

The same HPLC system was used to analyze the *Syzygium aromaticum* methanolic extract. The mobile phase used consisted of water (40%, v/v), methanol (10%, v/v), and acetonitrile (50%, v/v), delivered at a flow rate of 0.7 mL/min in isocratic mode. All the other parameters were kept constant except for a 25 min run time.

Results and discussion

XRD

XRD patterns were obtained to study the crystallographic orientation of the synthesized materials (Fig. 1). The XRD pattern of chitosan shows a broad peak at 2θ, 19.47° representing the (110) crystalline plane with a d spacing of 0.46 nm and a crystallite size of 5.13 nm with 11.26 crystallites (JCPDS card no:39–1894). The XRD pattern of CuO shows peaks at 32.52°, 35.59°, 38.78°, 48.82°, 53.64°, 58.24°, 61.51°, 66.41° and 68.20° corresponding to (110), (002), (111), (–202), (020), (202), (–113), (–311) and (220) crystalline planes (PDF card no: 48–1548) with interlayer distances of 0.27, 0.25, 0.23, 0.19, 0.17, 0.16, 0.15, 0.14, and 0.14 nm, respectively with the crystallite size of 16.88 nm and 67 crystallites. The respective peaks of chitosan and CuO were present in all nanocomposites, with the peak corresponding to (110) crystalline plane of chitosan being less intense in nanocomposites with varying CuO load, and the same peak increased in intensity with increasing proportion of chitosan in nanocomposites in which CuO is kept constant. Interestingly, in the Chi:CuO 2:1, 3:1, and 4:1 nanocomposites, a new peak appeared in general at 36.52°, the intensity of which increased with the increasing weight proportion of chitosan. This peak corresponds to the (111) crystalline plane of Cu_2O (ICDD No:01–078-2076), suggesting that with the growing proportion of chitosan in the nanocomposite, Cu^{2+} in CuO lattice reduces to Cu^{+}, and hence, Cu_2O is produced. Donations of lone pair electrons on the NH_2 groups of chitosan to the Cu^{2+} centers facilitate the reduction. Increasing the proportion of chitosan and hence, NH_2 groups reduce

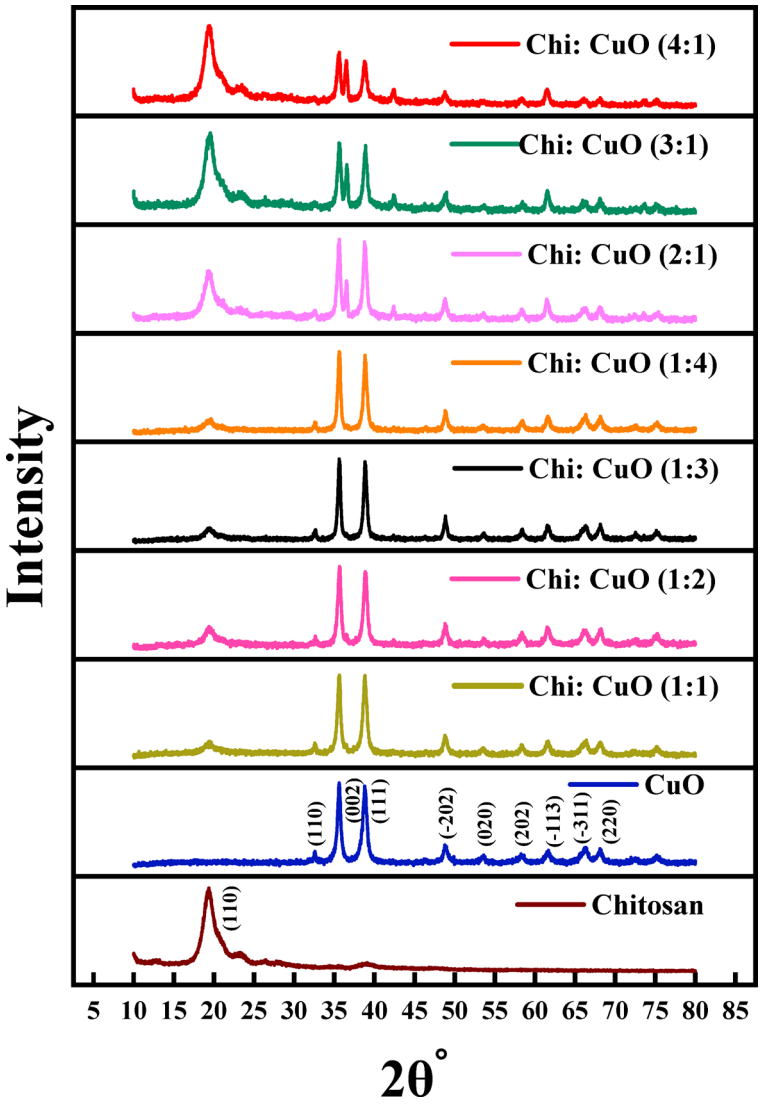

Fig. 1. The XRD patterns of synthesized materials.

more Cu^{2+}, producing more Cu_2O, giving rise to the corresponding characteristic peak with increasing intensity. It is interesting to note that the crystallite size of Cu_2O decreased as in 30.57 nm, 23.38 nm, and 20.90 nm, and the number of crystallites decreased as in 127.38 nm, 95.22 nm, and 84.92 nm with an increasing proportion of chitosan as in Chi:CuO 2:1, 3:1, and 4:1 in chitosan/CuO nanocomposites. The same trend was observed in both parameters above discussed with Cu_2O in CuO. The crystallite size, which was 17.39 nm in Chi:CuO 1:1, was decreased as 16.05 nm, 15.02 nm, and 15.05 nm in Chi:CuO 2:1, 3:1, and 4:1 nanocomposites, and the number of crystallites, which was 69.05 nm in Chi:CuO 1:1 was decreased as 63.73 nm, 59.67 nm and 59.67 nm in those nanocomposites, respectively. This suggests that both the crystallite size and the number of crystallites reduce during the reduction of CuO and formation of Cu_2O with increasing proportion of chitosan. The crystallographic parameters of the synthesized materials are tabulated in Table 2.

Raman spectroscopic analysis

Raman spectra were collected to confirm the crystallography and to further study the vibrational modes present in the synthesized nanocomposites. Figure 2 Shows the Raman spectra of CuO and Chitosan:CuO 1:4. The Raman spectrum of CuO shows three main vibrational bands centered at 284, 328, and 618 cm^{-1} corresponding to the A_g, B_g and B_g vibrational modes of CuO[65]. The same in the spectrum of Chitosan:CuO 1:4 appear at 293, 318 and 623 cm^{-1}, respectively, where the first and third bands have been shifted to longer Raman shifts while the second band shifted to a lesser Raman shift, indicating the change in the vibrations once coupled with chitosan due to the formation of new interactions.

SEM and TEM analysis

SEM images of the synthesized materials were obtained to study the 3D surface morphology (Fig. 3). The SEM image of chitosan (Fig. 3a) shows an oval-shaped well-established macropore structure but with two different size distributions. Chitin, during the conversion to chitosan, is first treated with a mineral acid to remove the embedded and surface $CaCO_3$. The resulting powder is then washed with 3% NaOH to remove proteins, followed by washing it with 50% NaOH to facilitate the deacetylation. Hence, it is evident that the holes of two different sizes have been produced due to the removal of $CaCO_3$ and proteins. The SEM image of CuO (Fig. 3b) shows the random distribution of CuO nanorods arranged to different 3D geometries during the hydrothermal treatment. In addition to the nanorods, some irregularly shaped CuO structures were also observed in the SEM image of Chitosan: CuO 1:2 (Fig. 3c), and the porous structure of chitosan was not observed due to the deposition of CuO on the matrix surface.

Sample	Crystal plane	2θ°	L (nm)	d (nm)	L/d
CuO	002	35.59	16.89	0.25	66.99
	111	38.78	12.33	0.23	53.14
Chitosan	110	19.47	5.13	0.46	11.26
Chi:CuO (1:1)	110	19.36	4.67	0.46	10.18
	002	35.61	17.39	0.25	69.05
	111	38.79	13.26	0.23	57.14
Chi:CuO (1:2)	110	19.37	4.93	0.46	10.77
	002	35.65	15.78	0.25	62.71
	111	38.87	14.00	0.23	60.49
Chi:CuO (1:3)	110	19.33	5.10	0.46	11.10
	002	35.63	19.89	0.25	79.01
	111	38.82	16.25	0.23	70.10
Chi:CuO (1:4)	110	19.36	4.78	0.46	10.43
	002	35.63	18.84	0.25	74.83
	111	38.80	14.82	0.23	63.91
Chi:CuO (2:1)	110	19.45	5.30	0.46	11.63
	002	35.62	16.05	0.25	63.73
	(Cu_2O) 111	36.52	30.57	0.24	127.38
	111	38.78	15.34	0.23	66.13
Chi:CuO (3:1)	110	19.57	5.34	0.45	11.78
	002	35.64	15.02	0.25	59.67
	(Cu_2O) 111	36.56	23.38	0.25	95.22
	111	38.84	14.11	0.23	60.91
Chi:CuO (4:1)	110	19.45	5.82	0.46	12.77
	002	35.56	15.05	0.25	59.67
	(Cu_2O) 111	36.48	20.90	0.25	84.92
	111	38.81	13.40	0.23	57.79

Table 2. Crystallographic parameters of the synthesized materials.

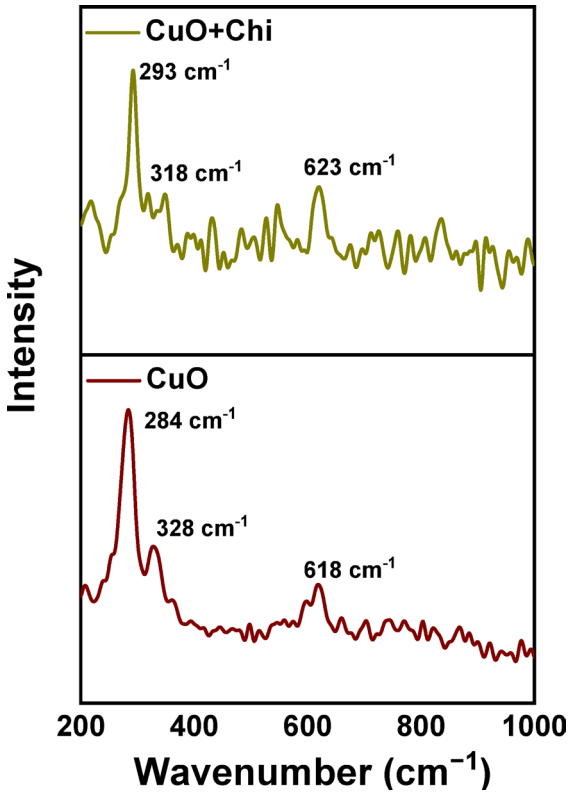

Fig. 2. Raman spectra of the synthesized materials.

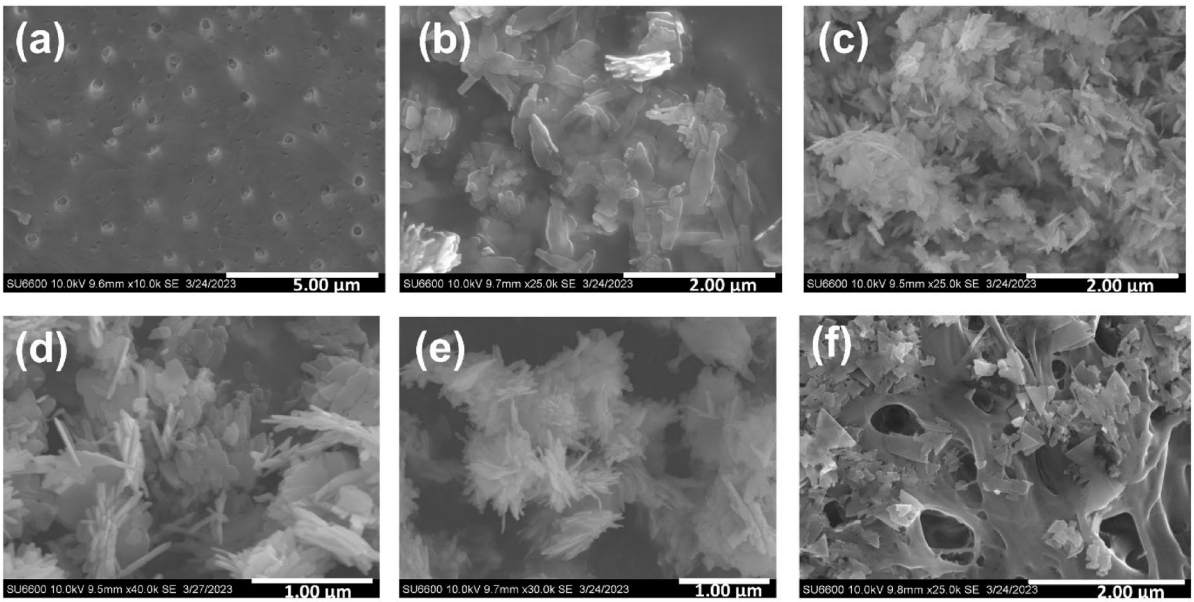

Fig. 3. SEM images of the synthesized materials (**a**) Chitosan (**b**) CuO (**c**) Chi:CuO (1:2) (**d**) Chi:CuO (1:4) (**e**) Chi:CuO (2:1) (**f**) Chi:CuO (4:1).

The irregular structures of CuO have been produced due to the Oswald ripening that occurs during the hydrothermal treatment, where CuO growth occurs in different directions. They have not grown to produce a specified 3D structure due to the insufficiency of CuO on the chitosan surface. This observation is quite further evident in the SEM image of Chitosan:CuO 1:4 as well (Fig. 3d). However, in the SEM image of Chitosan:CuO 2:1 (Fig. 3e), more nanorods arranged protruding to different directions from a common center were observed abundantly with comparatively lesser irregularly shaped CuO. This could be due to the presence of more chitosan

providing more active sites for CuO to be anchored during the hydrothermal process and pressure being applied in many directions, facilitating the growth of CuO along those directions due to Oswald ripening. An interesting morphology was observed in Chitosan:CuO 4:1 (Fig. 3f). The macropore structure of chitosan was quite visible due to the high proportion of chitosan present in the nanocomposite, and CuO has been developed as triangles during the hydrothermal treatment, and they are distributed in the macropore structure. Additionally, there were some irregularly shaped structures with few nanorods. The TEM image of the same nanocomposite shown in Fig. 4a also shows the predominantly present triangle-shaped structures, and the presence of fewer nanorods entrapped in the larger triangle structures is shown in Fig. 4b.

XPS analysis

XPS spectra were collected to study the surface chemistry of the synthesized materials. Survey spectra were collected to identify the elements present on the surface of the materials, while the higher resolution spectra were obtained to identify the different chemical environments an element would exist specifically. Survey spectra of Chitosan, CuO, Chi: CuO 1:2, Chi: CuO 1:4, Chi: CuO 2:1 and Chi: CuO 4:1 are given in Figure S1a–f, respectively. The survey spectrum of Chitosan shows the presence of C, O, and N as the main elements, and the survey spectrum of CuO shows the presence of Cu, C and O. The Chitosan-CuO nanocomposites generally show the presence of C, O, N and Cu. The presence of N was not identified in the survey spectra of Chi: CuO 1:2 and Chi: CuO 1:4 because proportionally, N-bearing chitosan is present in low amounts compared to the CuO in the nanocomposite.

The higher resolution spectrum of C 1s of chitosan shown in Fig. 5a is deconvoluted to five peaks at 284.5, 285.1, 286.0, 286.6 and 288.0 eV, which are attributed to C=C, C=N, C–O, C–N or C≡N and C=O bonds, respectively. Three peaks appeared in the higher resolution C 1s spectrum of CuO (Fig. 5b) at 284.5, 285.6 and 288. eV, representing the C=C, C–O and C=O bonds, respectively. The N 1s higher resolution spectrum of Chitosan exhibited in Fig. 5c is deconvoluted to two peaks at 399.5 and 400.1 eV, assigned to pyrrolic nitrogen and hydrogenated nitrogen, respectively. The higher resolution spectra of N1s of Chi: CuO 1:2 and Chi: CuO 1:4 appeared to have a low signal-to-noise ratio due to the low amount of N-bearing chitosan present in the nanocomposite compared to CuO (Fig. 5d, e respectively). Further, due to the same reason, those two higher-resolution spectra could be deconvoluted into one peak only. However, the higher resolution spectra of N 1s of Chi: CuO 2:1 and Chi: CuO 4:1 shown in Fig. 5f, g respectively, were deconvoluted to two peaks showing the same bond nature discussed in Fig. 5c with a slight shift in the binding energy due to the presence of CuO which alter the chemical behaviour around N due to the established interactions between CuO and chitosan during the hydrothermal treatment. The higher resolution spectrum of O 1s of Chitosan shown in Fig. 5h is deconvoluted to three peaks at 531.4, 532.8 and 533.6 eV, which are ascribed to O = C–N, C–O–C and C–OH, respectively. The higher resolution spectrum of O 1s of CuO is deconvoluted to three peaks at 529.7, 531.1, and 532.9 eV (Fig. 5i), which are assigned to the binding energy of lattice oxygen in CuO lattice (Cu^{2+}–O^{2-}), binding energy for oxygen defects within the CuO matrix and oxygen bound to carbon on adsorbed residual carbon. The higher resolution spectra of O 1s of Chi: CuO 1:2, Chi: CuO 1:4, Chi: CuO 2:1 and Chi: CuO 4:1 were deconvoluted to four peaks as shown in Fig. 5j–m, respectively, showing the presence of two types of oxygen in CuO lattice and Oxygen bound to carbon in different ways as described above. The higher resolution spectrum of Cu 2p of CuO (Fig. 5n) shows the spin-orbital coupling. The $2p_{3/2}$ and $2p_{1/2}$ peaks are split, suggesting the presence of two different oxidation states, Cu^{+} and Cu^{2+}, where the lower binding energy corresponds to Cu^{+} and the higher binding energy represents Cu^{2+}. The respective satellite peaks of $2p_{3/2}$ and $2p_{1/2}$ were also present. This chemical environment around Cu was observed in Chi: CuO 1:2, Chi: CuO 1:4, Chi: CuO 2:1 and Chi: CuO 4:1 as well as shown in Fig. 5o–r, respectively.

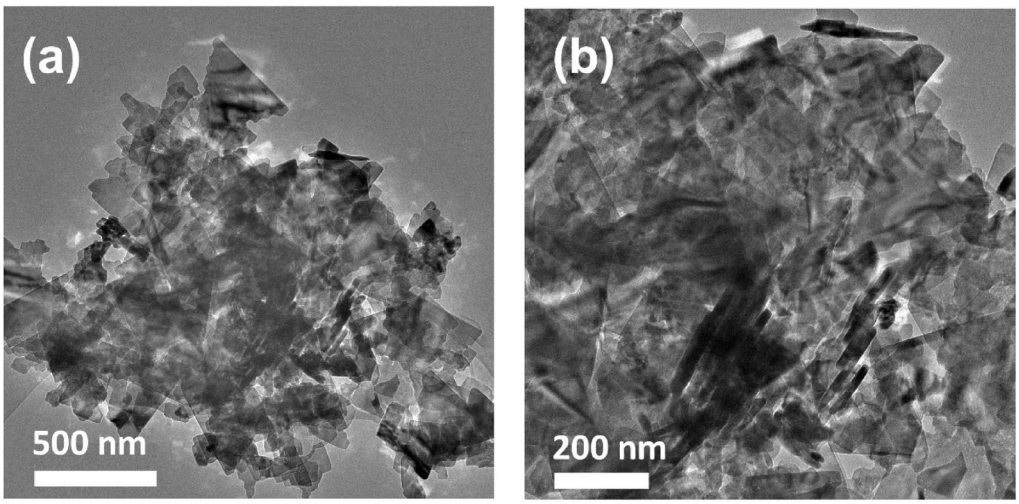

Fig. 4. TEM images of the synthesized materials (**a**) and (**b**) Chi: CuO (4:1).

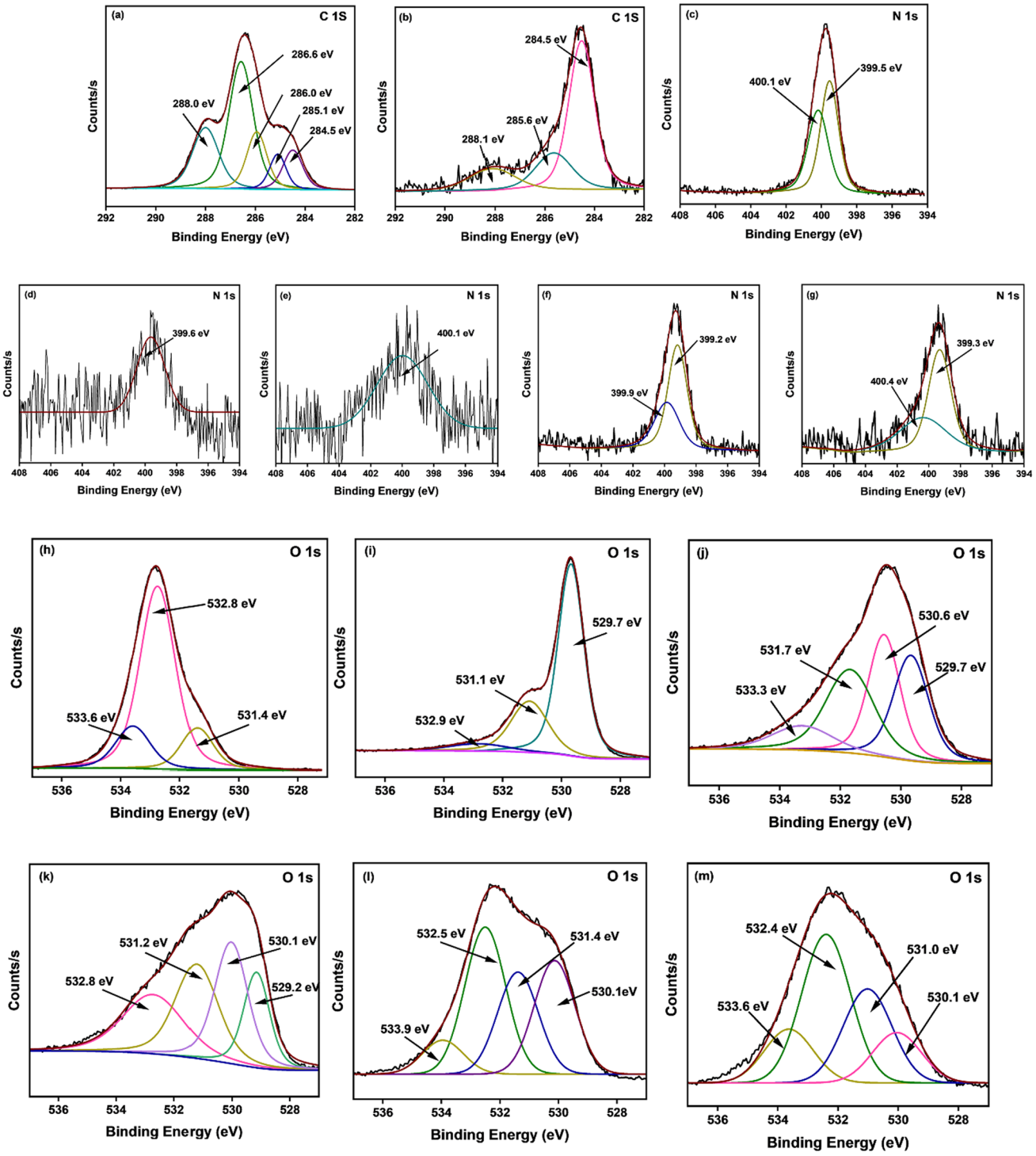

Fig. 5. The higher resolution spectra of C 1 s of (**a**) Chitosan (**b**) CuO, the higher resolution spectra of N 1 s of (**c**) Chitosan (**d**) Chi: CuO (1:2) (**e**) Chi: Cuo (1:4) (**f**) Chi: CuO (2:1) (**g**) Chi: CuO (4:1), the higher resolution spectra of O 1 s of (**h**) Chitosan (**i**) CuO (**j**) Chi: CuO (1:2) (**k**) Chi: CuO (1:4) (**l**) Chi: CuO (2:1) (**m**) Chi: CuO (4:1), the higher resolution spectra of Cu 2p of (**n**) CuO (**o**) Chi: CuO (1:2) (**p**) Chi: CuO (1:4) (**q**) Chi: CuO (2:1) (**r**) Chi: CuO (4:1).

FT-IR analysis

FT-IR spectra were collected to study the bonds present in the compounds fabricated and, more precisely, to determine the functionalization of the synthesized nanocomposites by the active compounds of the herbals, clove and Indian gooseberry Fig. 6. The FT-IR spectrum of chitosan exhibits a peak at 1308 cm^{-1}, which can be attributed to the C–O stretching frequency, and a peak at 1377 cm^{-1}, assigned to the O–H bending of the

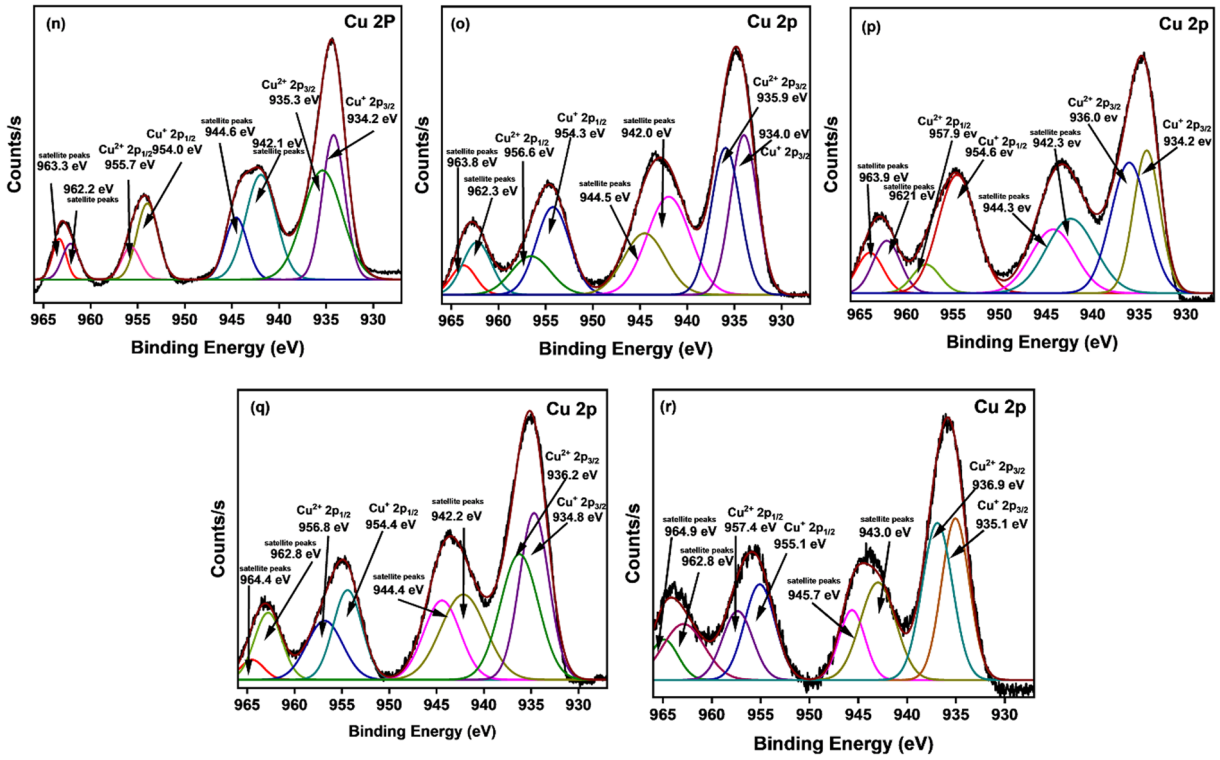

Fig. 5. (continued)

hydroxyl groups present in the structure. The peak at 1546 cm^{-1} can be attributed to the N–O stretching, and the peak at 1617 cm^{-1} represents the presence of C=C stretching. The C–H stretching is represented by the peaks present at 2878, 3100, and 3255 cm^{-1}, and the peak at 3447 cm^{-1} is ascribed to the N–H stretching of a primary amine present in the chitosan structure. The FT-IR spectrum of CuO nanoparticles shows peaks at 595 and 525 cm^{-1} that are attributed to the asymmetric and symmetric Cu–O stretching, confirming the presence of crystalline CuO. This confirms the formation of CuO nanoparticles. The peak at 869 cm^{-1} corresponds to Cu–O–H vibration, and the peaks at 1122 cm^{-1} and 1086 cm^{-1} are due to the C–O stretching vibration. The same bonds of chitosan spectra were present in the Chi:CuO (1:1) structure, though the peak positions vary slightly due to the coupling of chitosan with CuO. However, the corresponding peaks of Cu–O stretching were not present in the Chi:CuO (1:1) spectrum due to the signal masking, overlapping the strong absorption bands of chitosan with Cu–O vibrations in the low wavenumber region. The FT-IR spectrum of *P. emblica* extract-coated Chi:CuO shows different peaks. The peak at 1198 cm^{-1} is ascribed to the C–O stretching of substituted alcohol, and the peak at 1324 cm^{-1} represents the O–H bending frequency of alcohol. The peak at 1447 cm^{-1} is assigned to the C–H bending, and the peak at 1604 cm^{-1} represents the C=C stretching in αβ-unsaturated ketones. The peak at 1707 cm^{-1} is attributed to the C=O stretching, and the broad peak centered at 3237 cm^{-1} represents the O–H stretching. The same bonds were represented in the *S. aromaticum* extract-coated Chi:CuO, with slight variations in peak positions, as a different chemical compound had been coated. These chemical bonds are present in the active compounds in Indian gooseberry, which are ellagic and gallic acids and eugenol in clove, confirming the functionalization of the nanocomposite by the active ingredient. CuO peaks were not prominent in the spectra of coated composites due to the overshadowing effect of strong organic peaks on the Cu–O vibrations. Additionally, it exhibited a strong peak at 2929 cm^{-1} with a shoulder peak at 2852 cm^{-1}, which are attributed to strong N–H stretching and C–H stretching, respectively, resembling the presence of chitosan. The presence of bioactive compound-specific peaks alongside chitosan/CuO bands confirms successful loading.

HPLC analysis

The HPLC fingerprint of *P. emblica* methanolic extract was analyzed with the ellagic and gallic acid commercial standards (Figure S2). "Characteristic peaks" were defined by their relatively high intensity and good resolution in the HPLC fingerprints. According to the HPCL chromatogram Fig. 7, the retention times of the gallic and ellagic acids are 3.99 min and 24.15 min, respectively, which align with the retention time of the commercial standards. The presence of gallic acid and ellagic acid in *P. emblica* extracts is consistent with the previous studies as reported by Li et al.[66]. Similarly, *S. aromaticum* extract was analyzed with the eugenol commercial standard, and the component was identified at 4.63 min as eugenol after the comparison of retention times. Furthermore, the UV spectra of the extracts' peaks were compared to the standards to verify the identification's specificity. A number of additional distinctive peaks were also detected in the extracts, which could indicate the presence of additional phenolic chemicals.

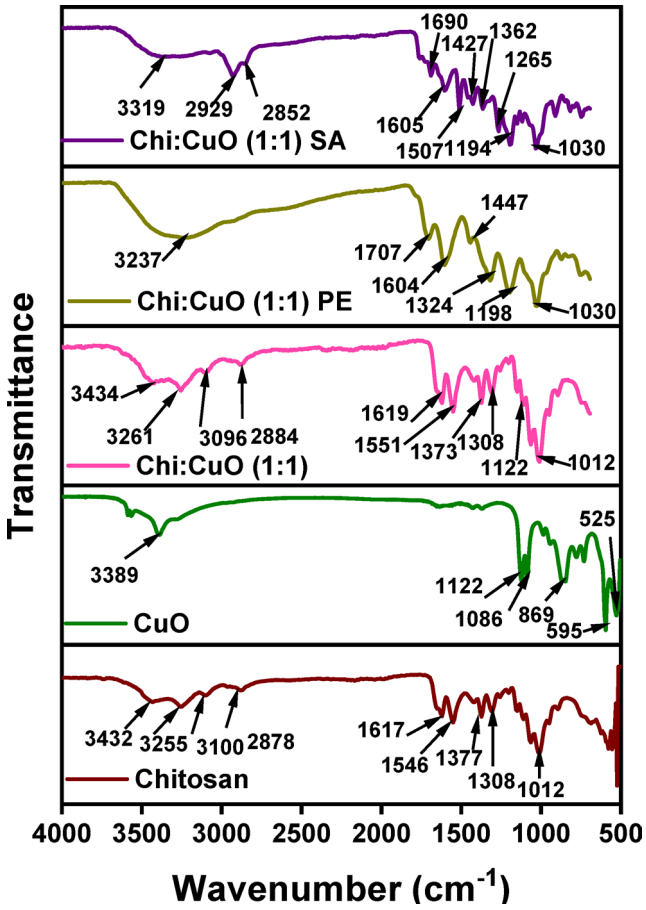

Fig. 6. FT-IR spectrum of the synthesized materials.

Phytochemical analysis

The observations of the experiment were similar for both solvents used in the experiment, according to the Table 3. Alkaloids, terpenoids, phenols, flavonoids, tannins, glycosides, steroids, and saponins were found to be present in both *Phyllanthus emblica* and *Syzygium aromaticum* extracts. *P. emblica* is a rich source of bioactive phytochemicals. Ellagic acid, gallic acid, and quercetin are prominent polyphenols in *P. emblica*[67]. These compounds exhibit strong anti-inflammatory, antioxidant[68], anticancer[69] and antibacterial[70] properties.

S. aromaticum is also a rich source of bioactive phytochemicals. Eugenol is the primary bioactive compound and is responsible for most of the biological activities[20], including the anti-inflammatory activity by inhibiting pro-inflammatory mediators like COX-2, LOX, TNF-α, and IL-6[71]. Eugenol disrupts bacterial cell membranes and inhibits biofilm formation while performing cell membrane homeostasis by protecting against lipid peroxidation and maintaining membrane integrity, which is crucial for triggering apoptotic responses[72]. Gallic acid is a polyphenolic compound that contributes to its antioxidant, anti-inflammatory, and anticancer activities. *S. aromaticum* contains hydrolyzable tannins, such as ellagitannins, which exhibit antibacterial and anticancer properties. Flavonoids like quercetin and kaempferol contribute to its anti-inflammatory and anticancer effects[20].

In addition to this, tannins have astringent characteristics, which speeds up tissue repair and inflammatory mucous membranes. These contain saponins, which have been proposed as potential anti-carcinogens[73]. The anti-carcinogenic actions of saponins have been linked to immune-modulatory effects and direct cytotoxicity. Similarly, it has been discovered that alkaloids, a broad class of secondary metabolites, possess antibacterial properties through the inhibition of DNA topoisomerase[20].

Antioxidant activity

The antioxidant activity of the methanolic extracts of *Phyllanthus emblica*, and *Syzygium aromaticum*, along with their chitosan-coated composites, was evaluated using the DPPH radical scavenging assay. According to the Fig. 8 the average radical scavenging ability of the *P. emblica* and *S.aromaticum* extracts and composite materials has shown a dose-dependent increment in the tested concentration range of 5–25 µg/mL. The percentage inhibition results across different concentrations revealed that *P. emblica* exhibited the highest radical scavenging activity, achieving 95.81% inhibition at 25 µg/mL, while *S. aromaticum* reached 89.06%. Interestingly, the chitosan composite of *P. emblica* showed improved inhibition at lower concentrations, with 45.36% inhibition at 5 µg/mL compared to 37.06% for the pure extract, suggesting an initial enhancement in bioactivity. However, at 25 µg/mL, the composite material showed a value of 94.88% for the scavenging ability, which was close to the value

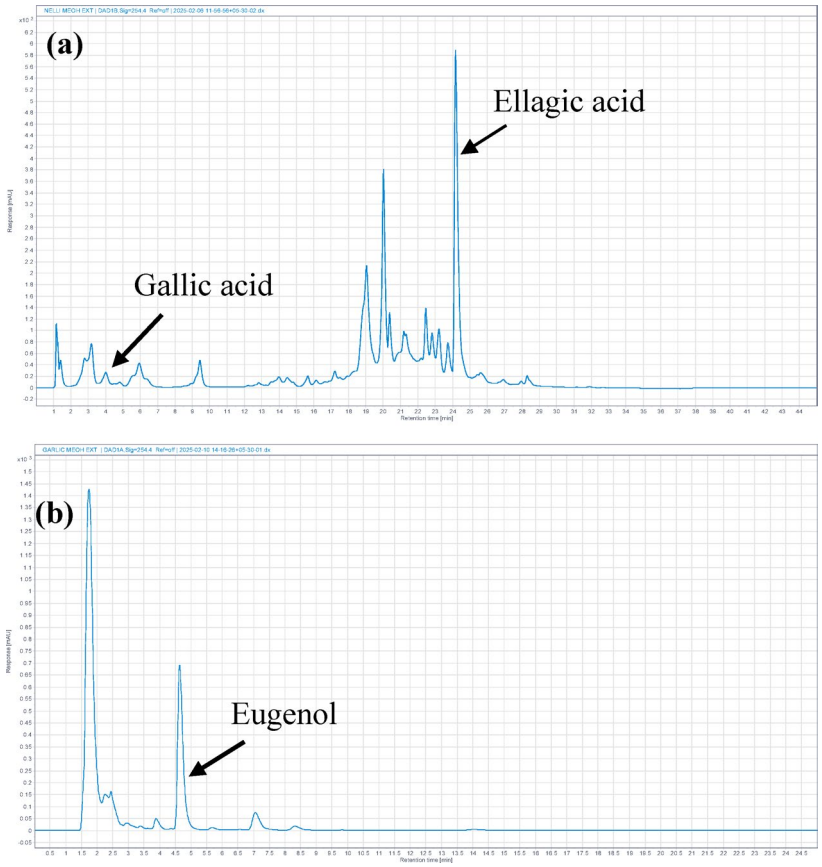

Fig. 7. HPLC fingerprint of (**a**)*P. emblica* extract (**b**)*S. aromaticum* extract.

Primary/Secondary metabolites in *Phyllanthus emblica*	Primary/Secondary metabolites in *Syzygium aromaticum*	Tests	Observation in methanol and water
Carbohydrates	Carbohydrates	Fehling's test	+
		Benedict's test	+
		Iodine test	–
Proteins	Proteins	Ninhydrin	–
Phenols and tannins	Phenols and tannins	Ferric chloride test	+
Flavonoids	Flavonoids	Alkaline reagent test	+
Saponins	Saponins	Frothing test	+
Glycosides	Glycosides	Salkowski's test	+
		Keller-Kilani test	+
Steroids	Steroids		+
Terpenoids	Terpenoids		+
Alkaloids	Alkaloids	Mayer's test	+

Table 3. Phytochemical analysis of the *P. emblica* and *S.aromaticum* methanolic extracts. Symbol (+) indicates the presence of the metabolite of interest, and Symbol (–) indicates the negative results.

reported for the *P. emblica* extract. In contrast, *S. aromaticum*-chitosan showed significantly lower inhibition, ranging from 19.75—58.98% at 5–25 µg/mL, indicating that chitosan encapsulation may have impeded the diffusion of active antioxidant compounds.

The IC_{50} values demonstrated that *P. emblica* exhibited the highest antioxidant activity (10.25 µg/mL), followed by *S. aromaticum* (12.08 µg/mL). The chitosan composites showed a reduction in half-maximal inhibitory concentration, with *P. emblica*-chitosan at 10.78 µg/mL, *S. aromaticum*-chitosan at 19.27 µg/mL, likely due to interactions between chitosan and active phytochemicals that may reduce free radical neutralization efficacy.

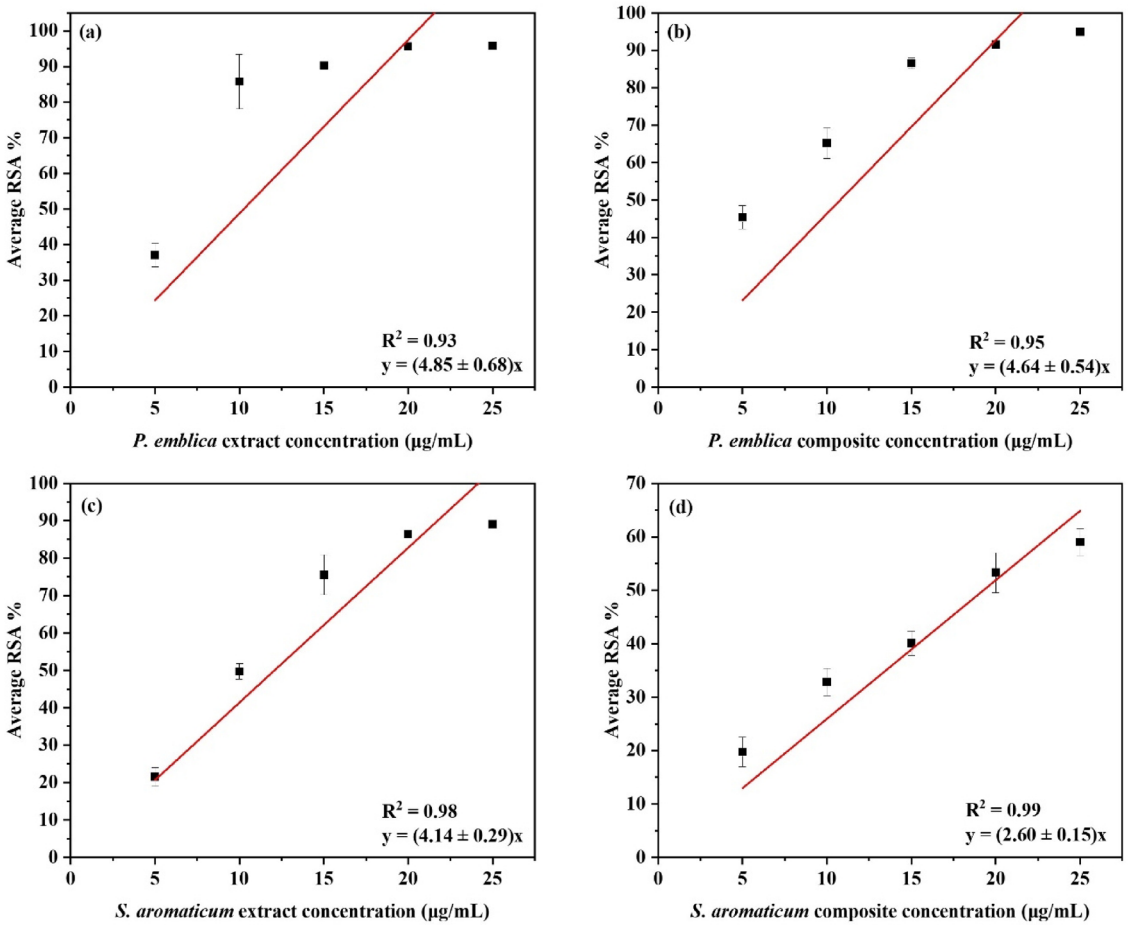

Fig. 8. DPPH radical scavenging ability of the (**a**)*P. emblica* extract (**b**)*P. emblica* extract coated chitosan composite (**c**) *S. aromaticum* extract (**d**) *S. aromaticum* extract coated chitosan composite.

The antioxidant activity of the samples was compared with ascorbic acid, a widely used positive control. Ascorbic acid exhibited an IC_{50} value of 4.21 µg/mL under the same experimental conditions, indicating superior radical scavenging activity compared to the plant extracts and composites (**Figure** S3). However, the activity of *Phyllanthus emblica* was notably close to that of ascorbic acid, highlighting its potential as a natural antioxidant source. The antioxidant activity of plant extracts can be attributed to their rich phytochemical composition, particularly phenolic compounds, flavonoids, and tannins, which are known to donate hydrogen atoms or electrons to neutralize free radicals[74]. Polyphenols, including phenolic acids (gallic acid) and flavonoids, are mainly responsible for their potent antioxidant activity in *P. emblica*[4].

Phyllanthus emblica, for instance, contains high levels of gallic acid, ellagic acid, and ascorbic acid, which contribute to its potent antioxidant properties. The major active ingredient in clove oil extract, eugenol, is a compound with an allyl group attached to a phenolic ring, which is responsible for antioxidant activity[75]. The slightly reduced activity of the chitosan composites may be due to the encapsulation of these bioactive compounds within the chitosan matrix, limiting their interaction with DPPH radicals. *Phyllanthus emblica* is renowned for its high vitamin C content and polyphenolic compounds, which have been extensively studied for their antioxidant, anti-inflammatory[4], and anticancer[76] properties. *Syzygium aromaticum* is rich in eugenol, a phenolic compound with strong radical scavenging activity. Chitosan's known ability to stabilize bioactive molecules could contribute to the altered antioxidant activity observed. While some studies report enhanced polyphenolic release in chitosan matrices[77,78], the present study suggests that polymeric interactions may reduce radical scavenging efficiency for certain extracts. Future research should focus on optimizing chitosan modification techniques to enhance the bioavailability of polyphenols while maintaining antioxidant efficacy.

The results of this study demonstrate that *Phyllanthus emblica* and its chitosan composite exhibit the highest antioxidant activity among the tested samples, followed by *Syzygium aromaticum*.

Anti-inflammatory activity

In this study, the anti-inflammatory activity of two methanolic plant extracts *Phyllanthus emblica*, and *Syzygium aromaticum*, their chitosan composites were investigated. The results demonstrated concentration-dependent inhibition of protein denaturation for all samples (Fig. 9). *Phyllanthus emblica* exhibited significant anti-inflammatory activity, with percentage inhibition ranging from 19.45% at 100 µg/mL to 70.17% at 700 µg/mL.

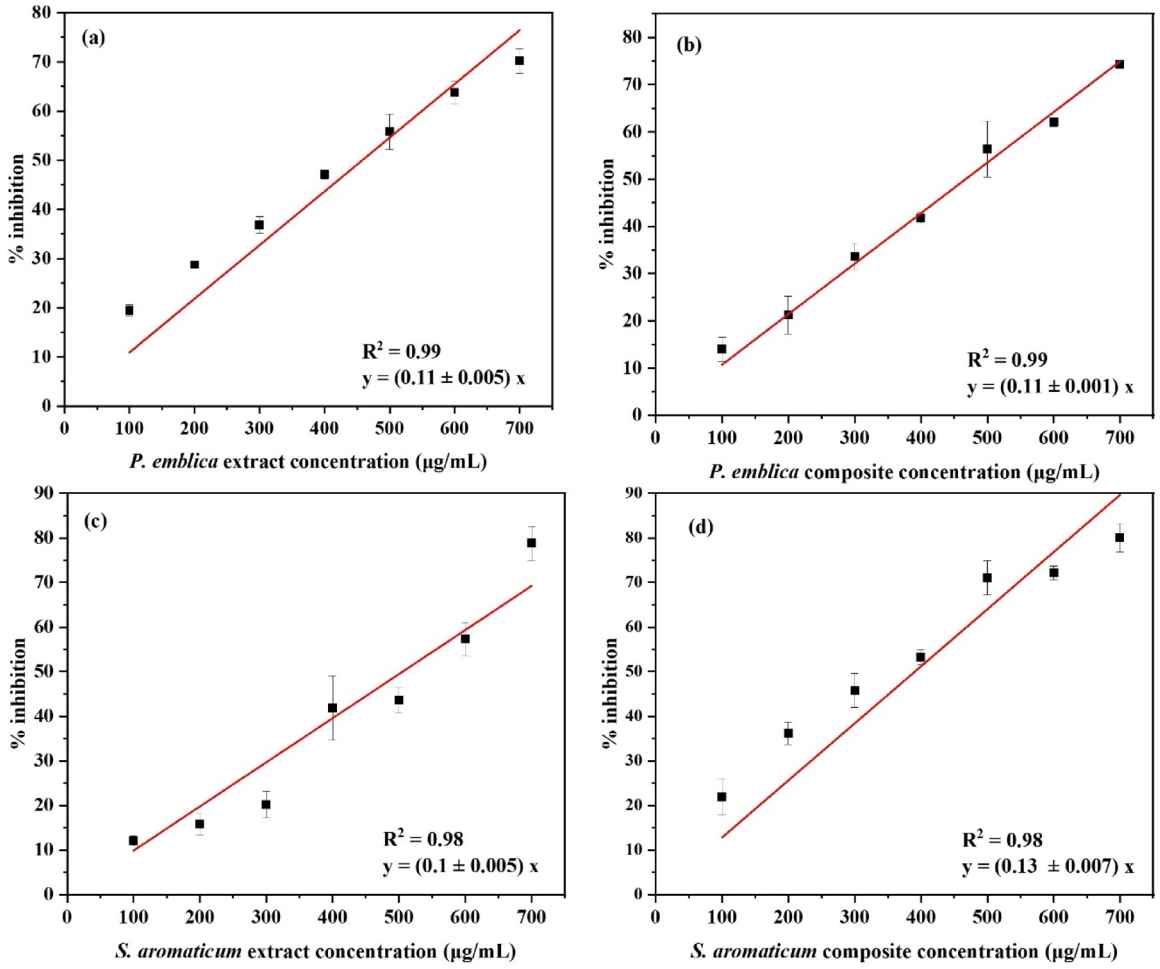

Fig. 9. Egg albumin denaturation inhibition activity of the (**a**)*P. emblica* extract (**b**)*P. emblica* extract coated chitosan composite (**c**) *S. aromaticum* extract (**d**) *S. aromaticum* extract coated chitosan composite.

In the concentration range between 100 and 700 µg/mL *P. emblica* composite material's protein denaturation inhibition was in the range between 13.98 and 41.74%, where percentage inhibition values were lower than that of *the P. emblica* extract. Even though the chitosan composite showed slightly lower activity at lower concentrations it showed a 74.29% inhibition at 700 µg/mL. *Syzygium aromaticum* and its composite displayed moderate activity, with the composite outperforming the pure extract at higher concentrations. *S. aromaticum* extract showed a high percentage inhibition activity of 78.80%, while the composite material exhibited a slightly higher value of 80.01% at the same concentration of 700 µg/mL, indicating an enhancement in the protein stabilizing ability of the composite material.

The IC_{50} values further highlighted the differences in anti-inflammatory efficacy. *Phyllanthus emblica* had the lowest IC_{50} value (458 µg/mL), indicating its superior activity, followed by *Syzygium aromaticum* (505.46 µg/mL). Interestingly, the chitosan composite of *Syzygium aromaticum* exhibited a lower IC_{50} value (390.44 µg/mL) than its pure extract, suggesting enhanced anti-inflammatory activity due to the chitosan matrix. In contrast, the composites of *Phyllanthus emblica* slightly higher IC_{50} values (467 µg/mL), indicating a marginal reduction in activity.

The anti-inflammatory activity of the samples was compared with diclofenac sodium, a standard non-steroidal anti-inflammatory drug (NSAID). Diclofenac sodium exhibited an IC_{50} value of 120.5 µg/mL under the same experimental conditions, demonstrating significantly higher activity than the plant extracts and composites. However, the activity of *Phyllanthus emblica* and its composite was notable, suggesting their potential as natural alternatives for controlling inflammation.

Phenolic compounds, flavonoids, and tannins present in *Phyllanthus emblica* and *Syzygium aromaticum* are known to interact with proteins, preventing their conformational changes[79] under heat stress. Additionally, these compounds may inhibit cyclooxygenase (COX) enzymes[80,81], which play a key role in the inflammatory pathway by catalyzing the synthesis of prostaglandins. *P. emblica* extract contains high content of gallic acid, ellagic acid and ascorbic acid[82], which is related to its superior anti-inflammatory activity[83]. Similarly, *S. aromaticum* is rich with eugenol, a phenolic compound with potent anti-inflammatory and analgesic effects[20]. Chitosan, on the other hand, has been reported to exhibit anti-inflammatory activity by modulating immune responses and reducing

the production of pro-inflammatory cytokines[84]. The enhanced activity of the *Syzygium aromaticum* composite may be due to synergistic interactions between the bioactive compounds in the extract and the chitosan matrix.

The results of this study demonstrate that *Phyllanthus emblica* and its chitosan composite exhibit the highest anti-inflammatory activity among the tested samples, followed by *Syzygium aromaticum*. The incorporation of chitosan enhanced the activity of *Syzygium aromaticum*, while it had a marginal inhibitory effect on the other extract. These findings highlight the potential of *Phyllanthus emblica* and *Syzygium aromaticum* as natural anti-inflammatory agents and suggest that chitosan-based composites could be further optimized for therapeutic applications.

Total phenolic content

The total phenolic content (TPC) of the *Phyllanthus emblica* and *Syzygium aromaticum* extracts and coated composites was determined using the Folin-Ciocalteu method. Gallic acid was used as the standard, and a calibration curve was constructed with concentrations ranging from 10 to 70 µg/mL. The standard curve exhibited a strong linear relationship, with the equation $y = 0.002\ x + 3.66E\text{-}5$ and an R^2 value of 0.99, indicating excellent linearity and reliability for quantification (Figure S4).

The TPC values for the extracts and their chitosan-coated composites are summarized in Table 4. TPC in the test sample was calculated using the regression equation, and it is reported as x. This value was converted to mg GAE/g to determine the TPC of the dry extract[85]. The results revealed slight variations in phenolic content across the samples, reflecting differences in their chemical composition and the efficiency of the hydrothermal coating process. For the analysis of the test samples, they were diluted 100 times to obtain the test solution with 10 µg/ml concentration from the 1 mg/mL stock solution.

The TPC of the *Phyllanthus emblica* extract was 45.43 mg GAE/g, while the *P. emblica* coated chitosan composite showed a slightly higher value of 45.63 mg GAE/g. The values reported for the phenolic content are consistent with previous studies[86] reporting that *Phyllanthus emblica* is rich in polyphenolic compounds, such as gallic acid, ellagic acid, and flavonoids, which contribute to its strong antioxidant activity. The *S. aromaticum* extract was reported to have a TPC of 45.47 mg GAE/g, which is consistent with literature[87]. Similarly, its' coated composite exhibited slightly higher TPC values of 45.78 mg GAE/g. The coating process slightly enhanced the phenolic content compared to the pure extract.

The *Syzygium aromaticum* extract and the composite material showed similar variations in TPC values to that of the *P. emblica* samples. This is consistent with the known presence of eugenol, gallic acid, and other phenolic compounds in clove extracts, which contribute to their strong antioxidant properties. The high TPC values suggest that *Syzygium aromaticum* is a potent source of natural antioxidants. The hydrothermal treatment of chitosan likely enhanced its ability to form stable complexes with phenolic compounds, thereby improving their stability and bioavailability[88]. This is supported by recent studies demonstrating that hydrothermally treated chitosan exhibits improved mechanical properties and enhanced interaction with bioactive compounds[89]. The increased TPC values observed for the chitosan-coated composites suggest that hydrothermal treatment could be a promising strategy for enhancing the functional properties of plant extracts.

Drug release kinetics

In this study, extracts of *Phyllanthus emblica* and *Syzygium aromaticum* have shown significant antioxidant, anti-inflammatory, and antibacterial activities as determined by the DPPH assay, egg albumin denaturation assay, and antimicrobial assays. Further, the presence of the bioactive compounds of ellagic acid, gallic acid, and eugenol was confirmed through the HPLC analysis. As described, they exhibit remarkable antimicrobial, antioxidant, anti-inflammatory, and anticancer properties. Therefore, drug delivery studies were carried out using plant extracts coated chitosan composites to ensure the sustained release of the bioactive compounds, namely gallic, ellagic acids, and eugenol, by improving bioavailability, therapeutic efficacy, and stability. Chitosan is a widely used biopolymer in drug delivery studies in various aspects. Rajaei et al.[90] and Lohiya & Katti[91] have reported the usage of chitosan/agarose/graphene oxide nanohydrogel and carboxylated chitosan/mesoporous silica nanoparticle-based drug delivery systems as a treatment option for breast cancer, respectively. Furthermore, a delivery system composed of porous chitosan microspheres and hydroxypropyl chitin hydrogel was used by Ji et al.[92] as a treatment for cartilage repair by macrophage immunomodulation. A study on curcumin release from chitosan/agarose/graphitic carbon nitride nanocomposite was reported by Rajabzadeh-Khosroshahi et al.[93] as a potential anticancer therapy. Moreover, chitosan-based delivery systems have been used for the delivery of plant bioactive compounds of *Spondias pinnata*, *Peganum harmala*, *Curcuma longa*, *Olea europaea* by Gomathi et al., Homayouni Tabrizi, Wijayawardana et al., and Katouzian & Taheri[94–97]. Even though the above-mentioned extracts coated CuO/chitosan composites were synthesized, they were not used in drug release analysis, due to the potential cytotoxicity of CuO[98,99], which could cause health safety concerns, compromising the therapeutic usage. Drug release kinetics studies were carried out, varying the pH and ionic strength of the release media,

Source	Absorbance	*x* (µg GAE/mL)	Dilution Factor	TPC in dry extract (mg GAE/g)
Phyllanthus emblica extract	0.686	454.28	100	45.43
Phyllanthus emblica composite	0.689	456.27	100	45.63
Syzygium aromaticum extract	0.687	454.72	100	45.47
Syzygium aromaticum composite	0.691	457.82	100	45.78

Table 4. Total phenolic content of the synthesized materials.

and further changing the concentration of the drug. In healthy tissues, the extracellular environment normally maintains an ionic strength that is principally controlled by physiological NaCl concentrations[100] (~ 0.15 M) and a pH range of 7.35 to 7.45[101]. However, the extracellular environment shows notable abnormalities in malignant tissues and some disease situations, such as an acidic pH and variable ionic strength[102], because of altered ion homeostasis. Such conditions can affect the release kinetics and the efficacy of release of the active compounds. Concentrations above 0.5 M were not considered to be tested for the possibility of producing non-representative drug release profiles, as they exceed the in vivo physiological conditions[103]. Furthermore, polymer instability or precipitation due to extremely high ionic strengths can make it more difficult to interpret the results[104]. Therefore, a range of pH levels (pH 1–10) and NaCl concentrations (0.1–0.5 M) were selected to stimulate the physiological and pathological conditions of the extracellular matrix, to study the release pattern of the ellagic acid, gallic acid, and eugenol from the chitosan biopolymeric delivery system.

According to the CDR% data, *Phyllanthus emblica* coated chitosan biopolymer (*PeC*) and *Syzygium aromaticum* loaded chitosan biopolymer (*SaC*) have shown variations in release profiles based on the media conditions. The release profile of *PeC* in pH 1 has the highest release with a burst effect, which is attributed to the protonation of NH_2 groups of chitosan and phenolic and carboxyl groups of ellagic and gallic acid. The NH_3^+ groups create electrostatic repulsion forces between the chains, resulting in swelling of the polymer matrix. Gallic and ellagic acid exhibit better solubility under acidic conditions, which allows a rapid diffusion of the loaded bioactive compounds with the swelling of the matrix. However, in the media with pH 2.5–5.5, the CDR% has been reduced, even though the chitosan remains protonated, but swelling has been reduced compared to the pH 1 media. Further, ellagic acid (pKa = 5.6) and gallic acid (pKa = 4.4) start deprotonating, creating electrostatic interaction with the NH_3^+ groups, reducing the release. In the neutral media conditions (pH 7 -7.4), the release has been decreased further due to the deprotonation of chitosan (pKa = 6.7), leading to forming an insoluble polymer matrix. At alkaline conditions (pH 8.5–10), the release was shown to be lower, as the combined effect of chitosan deprotonation lowers the solubility of the polyphenols. Eugenol in *SaC,* being a weakly acidic, hydrophobic molecule with minimal ionization (pKa = 10.2), does not form electrostatic bonds with the matrix. However, the release at pH 1 media is higher due to the swelling of the chitosan, and the optimal release is reached in the media with pH 5.5. The balanced state between polymer swelling and diffusion occurs here with the partial protonation and free diffusion of non-ionised eugenol. When the pH increases (pH 7–10) polymer starts collapsing with losing the positive charge, making the matrix more hydrophobic. But more hydrophobic eugenol release from the shrunken matrix due to thermodynamic push, supported by the weak van der Waals interactions with chitosan, unlike the H-bondings of ellagic and gallic acid. Eugenol remains neutral in alkaline conditions, and the hydrophobic forces govern the gradual release (pH 8.5–10).

The release of *PeC* has decreased with the increase of the ionic strength of the media, due to the shielding of the chitosan's NH_3^+ groups, which makes the polymer more hydrophobic. Even though the release of gallic and ellagic acid can occur in lower ionic strengths (0.1–0.2 M), with the slight swelling of the polymer. Cl^- can compete with the carboxyl and phenolic groups and bind with the NH_3^+ groups, allowing the release of polyphenols. In contrast, at higher ionic strengths, Na^+ and Cl^- ions shield the NH_3^+ groups and reduce the porosity of the matrix. This further decreases the water intake/swelling, trapping the polyphenolic compounds in the matrix. The increasing NaCl concentration was reported to act favorably with the release of *SaC*. In lower ionic strength media conditions, slight swelling of the chitosan can be expected with minimum shielding effects. This allows the release of active compounds via the temporarily loosened matrix. Similar to alkaline conditions, eugenol partitions out of the hydrophobic, shrunken polymer matrix, governed by the matrix porosity and hydrophobic partitioning. Moreover, the lack of H-bonding with the polymer matrix allows the efficient release of bioactive compounds.

At lower concentrations (2.5 mg), polyphenols of *PeC* are moderately dispersed on the chitosan matrix, and the release has exponentially increased when the concentration of the drug increases to 5 mg, exhibiting a concentration-driven release. It was reported that there were no observable differences in the release profile of 7.5 and 10 mg drug dosages, due to the saturating effect of chitosan binding sites. The excess drug will form clusters, creating a diffusion barrier. Conversely, eugenol tends to disperse molecularly in the matrix, creating weak van der Waals forces. Minimal saturation effects are present due to the absence of aggregation and weak polymer interactions, ensuring the sustained increase in release at higher concentrations. Therefore, *PeC* has displayed sustained release at acidic, low ionic strength and lower doses, whereas *SaC* exhibited increased release with higher ionic strength conditions, higher drug dosages and near neutral media compositions. However, drug composites (*PeC* and *SaC*) were reported to have an improved release under physiological conditions (pH 7.4, 0.1–0.2 M NaCl) via different mechanisms.

Mathematical models are employed to understand the release mechanisms that help with the sustained release. The models will yield drug kinetic release parameters that can be used in developing an improved release process. Furthermore, they can be used to compare and correlate the release mechanisms using different models[105]. Drug release from chitosan bioplymeric delivery systems has been extensively studied in the literature using the Korsmeyer-Peppas model, Higuchi model[106,107], Hixson-Crowell model[108], Zero-order[109], First order[110] and Peppas-Sahlin models[111]. In order to analyze the drug release, 60% of the release data were fitted into six kinetic models, namely: First order, Zero Order, Higuchi, Korsmeyer Peppas, Peppas–Sahlin, and Hixson–Crowell models, respectively. The rate at which the drug is released from the delivery mechanism determines the drug dosage rate in sustained drug release systems. The drug's release kinetics are described by the rate constant (k) derived from the kinetic models. It is also employed to optimize different formulations to attain the intended release profile and to compare the release rates of different formulations. In the same way, the release exponent (n) is a significant kinetic parameter that indicates the drug release mechanism. It offers information about how the drug and environment interact, which helps create formulations with particular release properties[112]. Tables S1-S6 summarize the model parameters along with the R^2values of the model that fits. Based on the R^2 values,

the best fitted kinetic models were selected to interpret the release mechanism of the bioactive compounds of the plant extracts from the chitosan biopolymer. The models that exhibited $R^2 \geq 0.96$ were used to determine the controlled drug release mechanisms underlying the release of the bioactive compounds. In most cases, Korsmeyer Peppas and Peppas–Sahlin models were fitted well ($R^2 \geq 0.96$) with the experimental cumulative drug release percentage of the drug composite materials, as shown in the Table 5. The other models, specifically First Order and Zero Order, showed relatively lower R^2 values ($R^2 < 0.96$) in all the drug composites under the varying experimental conditions. Therefore, when interpreting the results, those models were not taken into consideration.

The release exponent, n, is a crucial parameter for classification in the Korsmeyer Peppas model (KP), which explains drug release processes that include both Fickian and non-Fickian behaviors. Pure Fickian diffusion is shown by $n = 0.43$, whereas quasi-Fickian diffusion is represented by $n < 0.43$. The mechanism indicates non-Fickian diffusion, which is defined by a combination of diffusion and swelling control, for values in the range $0.43 < n < 0.85$. Furthermore, the model corresponds to case II transport, which is mostly controlled by gel swelling, at $n = 0.85$. This theoretical framework offers a thorough comprehension of the various drug release patterns seen in polymeric systems[38].

Table 5 includes the diffusional exponent (n) and release constant (k_p) values of the bioactive compounds' diffusion from the chitosan biopolymer matrix. Figures S5 and S12 represent the non-linear curve fitting data of the plant extract-coated chitosan drug composites according to the Korsmeyer Peppas model. The R^2 value ($R^2 \geq 0.96$) indicates the suitability of the model to be used in the analysis and release exponent values are less than 0.43 in all cases which indicates the quasi-Fickian diffusion is responsible for the release of the bioactive compounds. In detail, *PeC* and *SaC* have indicated similarities in the model parameters. Release exponent (n) values of the *PeC* drug composite vary between 0.16–0.41, whereas the values for SaC drug composite are between 0.25–0.38. The *PeC* composite has shown a sustained release at pH 5.5–7.4 media compositions with higher release rates controlled by quasi-Fickian diffusion. However, in the media with pH 1, limited diffusional control can be observed with the higher initial burst effect in the polymer matrix. Diffusion persists in alkaline media conditions, but the increment in the n values suggests that the shrunken chitosan matrix has reduced the effect of diffusion on drug release. Media with 0.2 M NaCl show optimal release conditions with a lower n value and higher release rate, followed by moderate release at 0.1 M media with initial matrix loosening. The release rate has been reduced when the concentration increased to 0.3 M, and the release mechanism is closer to anomalous transport, with the hydrophobic collapse of the chitosan matrix masking the NH_3^+ groups. However, at 0.4 M media, the release was shown to be higher than in other media compositions, and the rate decreased

	pH 1	pH 2.5	pH 4	pH 5.5	pH 7	pH 7.4	pH 8.5	pH 10	0.1 M	0.2 M	0.3 M	0.4 M	0.5 M	2.5 mg	5 mg	7.5 mg	10 mg
Chitosan: *P. emblica* composite																	
Korsmeyer–Peppas model parameters																	
k_p	0.96	2.68	1.18	1.62	1.65	1.19	1.22	1.35	0.68	0.79	0.53	1.19	0.73	0.93	1.44	3.14	2.13
n	0.35	0.19	0.30	0.23	0.24	0.29	0.31	0.27	0.39	0.37	0.42	0.29	0.36	0.20	0.23	0.16	0.27
R^2	0.99	0.96	0.98	0.97	0.97	0.97	0.97	0.96	0.98	0.96	0.97	0.97	0.95	0.97	0.99	0.95	0.95
Peppas—Sahlin																	
k_D	0.63	0.93	0.71	0.77	0.95	0.72	0.72	0.81	0.53	0.56	0.50	0.70	0.54	0.53	0.75	0.96	0.82
k_R	0.44	0.77	0.55	0.63	0.81	0.56	0.55	0.66	0.33	0.37	0.32	0.55	0.37	0.44	0.61	0.80	0.78
m	0.21	0.17	0.18	0.16	0.15	0.17	0.20	0.17	0.23	0.22	0.22	0.18	0.20	0.12	0.15	0.17	0.20
R^2	0.99	0.96	0.98	0.97	0.97	0.97	0.97	0.96	0.98	0.96	0.97	0.97	0.95	0.97	0.99	0.95	0.96
Higuchi																	
k_H	0.41	0.43	0.35	0.33	0.36	0.34	0.41	0.36	0.36	0.37	0.32	0.34	0.31	0.16	0.30	0.43	0.55
R^2	0.99	0.94	0.98	0.95	0.97	0.97	0.97	0.96	0.98	0.95	0.96	0.96	0.93	0.93	0.97	0.93	0.96
Chitosan: *S. aromaticum* composite																	
Korsmeyer–Peppas																	
k_p	1.71	1.49	2.17	1.94	1.89	1.52	1.29	1.66	1.82	1.42	1.19	1.37	1.61	0.69	1.46	1.24	1.16
n	0.30	0.27	0.24	0.29	0.27	0.31	0.34	0.28	0.25	0.33	0.32	0.34	0.33	0.32	0.28	0.33	0.38
R^2	0.98	0.94	0.95	0.91	0.93	0.95	0.93	0.93	0.94	0.94	0.96	0.93	0.92	0.99	0.96	0.95	0.94
Peppas—Sahlin																	
k_D	0.91	0.76	1.05	0.73	0.80	0.75	0.71	0.78	0.86	0.73	0.71	0.78	0.69	0.47	0.75	0.73	0.62
k_R	0.87	0.60	0.96	0.74	0.68	0.63	0.59	0.64	0.72	0.63	0.54	0.73	0.69	0.32	0.59	0.58	0.59
m	0.18	0.18	0.16	0.21	0.19	0.20	0.21	0.19	0.18	0.21	0.20	0.20	0.22	0.19	0.19	0.20	0.23
R^2	0.98	0.93	0.94	0.91	0.91	0.94	0.93	0.91	0.92	0.94	0.96	0.93	0.91	0.99	0.96	0.95	0.94
Higuchi																	
k_H	0.52	0.39	0.48	0.57	0.49	0.50	0.50	0.47	0.43	0.51	0.42	0.53	0.59	0.24	0.40	0.46	0.57
R^2	0.96	0.89	0.90	0.88	0.88	0.92	0.91	0.88	0.88	0.91	0.94	0.90	0.89	0.98	0.93	0.93	0.93

Table 5. Drug release kinetics data of Chi: *P. emblica* and Chi: *S. aromaticum* composites fitted with Korsmeyer Peppas Model, Peppas Shalin model and Higuchi model (model parameters and R^2 values).

when the ionic strength increased to 0.5 M. The sudden increase is due to the salting-in effect of the matrix results from uneven dehydration, where some regions shrink, while others develop micropores, leading to the sudden enhancement in release rate. Salting-in effects dominate in 0.5 M media conditions, again reducing the release of polyphenols from the shrunken polymer matrix. Polyphenols are released via diffusion at low loading doses (2.5–5 mg), indicating a dose-dependent increase in the release. The highest release rate is recorded at the 7.5 mg concentration, which is reduced at the 10 mg concentration due to the saturation effect of the loaded polyphenols, as explained by the CDR% profiles. In acidic media conditions (pH 1–2.5), the release of eugenol from *SaC* is controlled via a moderate diffusion of the swollen matrix. When the pH is increased (4–7.4), optimal release conditions with balanced swelling and diffusion of hydrophobic eugenol happen, exhibiting the highest release rate at pH 4. With the increased alkalinity, n values were increased, suggesting the formation of transient pores with polymer rearrangements at pH 8.5, leading to the release of loaded bioactives via a combination of relaxation and diffusion. Nevertheless, these transient pores form stable hydrophobic nanochannels, leading to diffusion-like release in the fully hydrophobic chitosan matrix at pH 1 media. Similar to the *PeC*, *SaC* shows optimal diffusion rates at lower ionic strength media (0.1–0.2 M). With the shielding effects of higher Na^+ ions, the reduced repulsion between NH_3^+ groups creates partial shrinkage of the polymer matrix, creating heterogeneous pores. Hence, the rearrangements of the polymer cause the relaxational effects along with the diffusion of loaded bioactive compounds. At the highest ionic strength media, salting out effects predominantly expel eugenol from the completely collapsed, hydrophobic chitosan via the hydrophobic nanochannels. The impact of diffusion on release in 0.5 M media can be observed with a higher diffusion release rate compared to 0.3 M and 0.4 M media compositions. Initial lower k_p values at 2.5 mg drug concentration are due to the slow release, followed by a sustained release at the 5 mg concentration with optimal diffusion. At higher concentrations, diffusional contributions have become substandard as exhibited by increased n values, even though the release profiles were high in CDR% profiles. Thus, 5 mg concentration exhibited the optimal diffusional release rate. However, all the release mechanisms were controlled by the quasi-Fickian diffusion, with varying contributions of diffusion and relaxation at various media compositions. Molecules migrate from regions of high to low concentration in a process known as quasi-Fickian diffusion, which is similar to Fickian diffusion but takes into account other factors such as swelling or relaxing of the polymer matrix[113,114]. These variables cause the process to deviate from ideal Fickian behavior, suggesting that concentration gradients are not the only driving force. Rather, it is a system of diffusion and other processes that work together to affect molecular movement. This suggests that drug release is facilitated by the relaxation of polymer chains in chitosan or carrier surface degradation in addition to diffusion of the active ingredient (Fig. 10).

In the Peppas-Shalin(PS) model the contribution of the polymer relaxation and well as the diffusion (Fickian diffusion) are taken into consideration when deciding the drug release mechanism. The Fickian diffusional contribution (F) is represented by the second term in the model equation (Eq. 7), while the Case II relaxational contribution is represented by the right side[115]. The coefficient m stands for the strictly Fickian diffusion exponent in all systems with controlled release. If the bioactive compounds are released solely through the Fickian diffusion, the m value in the PS model should be equal to the n values obtained for the KP model. In *PeC* and *SaC* drug composites m and n values differ in all the media compositions (pH and ionic strengths) demonstrating that the polymer relaxation also contributes to the release of bioactive compounds other than the diffusion. As shown in Equation (Eq. 8) contribution of the polymer relaxation and diffusion for the release of bioactive compounds can be computed through the R/F ratio. All the model parameters are shown in Table 5 while Figures S11 and S18 represent the distribution of the R/F ratio of the PS model according to the cumulative drug release data obtained through the experiment for the chitosan coated *P.embica* composite and *S. aromaticum* composite, respectively. The release of the loaded drug is equally facilitated by diffusion and erosion when $R/F = 1$, with relaxation (erosion) predominating when $R/F > 1$ and diffusion predominating when $R/F < 1$[116].

According to Figures S10 and S17, the first 30 min of the drug release is aided by the diffusion ($R/F < 1$) of the bioactive compounds. In the latter phase of the release data, the R/F values have become higher ($R/F > 1$),

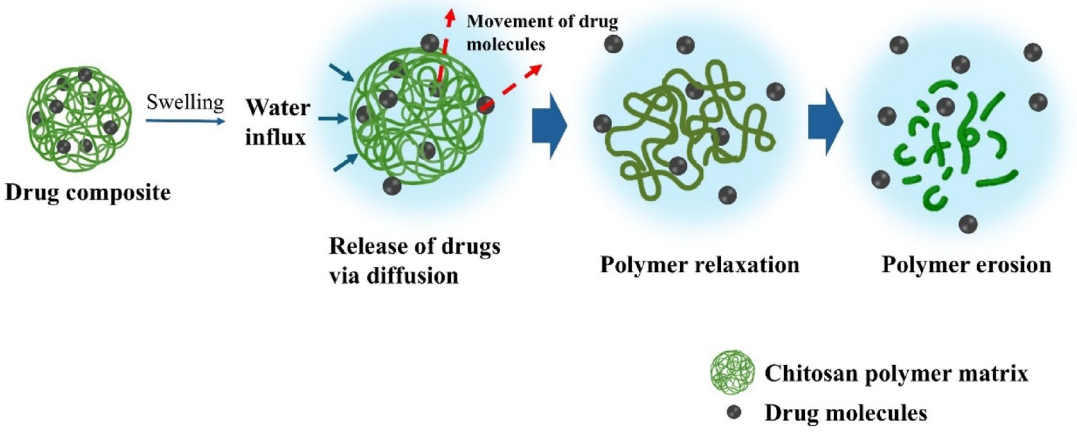

Fig. 10. Mechanism of release of the bioactive compounds from the chitosan biopolymeric delivery system.

indicating that the polymer relaxation has become the prominent release mechanism over time. Furthermore, drug release kinetics data of the KP model confirmed that the quasi-Fickian diffusion mechanism is responsible for the release of the bioactive compounds. Even though the diffusion is responsible for the release mechanism, the analysis demonstrated that purely Fickian diffusion did not facilitate the drug release from the chitosan biopolymeric system. This finding was additionally evident by the R/F values of the PS model, indicating that the polymer relaxation contributes significantly to the release of the bioactive compounds.

Figures S6 and S13 represent the non-linear curve fitting data of the plant extract-coated chitosan drug composites according to the PS model.In acidic media conditions (pH 1–4), diffusion-dominated release has contributed to the release of the polyphenols in *PeC* with higher k_D values and moderate k_R values, attributed to the chitosan matrix swelling at acidic conditions and relaxation governed by NH_3^+ group repulsions, respectively. At pH 5.5 balanced effect of diffusion and relaxation has been achieved in the swollen elastic matrix, reaching peak diffusion and relaxation contributions at pH 7. Diffusion is maintained at physiological pH conditions in the semi-rigid matrix, as the remaining NH_3^+ groups prevent the polymer from collapsing. Complete collapse of the chitosan matrix due to the formation of neutral NH_2 groups governs the diffusion of the coated drug compounds in alkaline pH (pH 10). Similar to the KP model release, in lower ionic strength conditions (0.1–0.3 M), diffusion dominates the drug release via the swollen chitosan pores in the matrix, with minimal chain mobility. However, in the media with 0.4 M NaCl, the relaxation contribution has increased with the formation of micropores due to the charge screening og NH_3^+ groups. But this impact from relaxation has decreased in 0.5 M media, with the complete collapse of the chitosan polymer blocking these transient pores. Lower drug loading has led to relaxed drug distribution, facilitating poor diffusional pathways (low k_P and k_D) at 2.5 mg concentration. At 7.5 mg concentration, optimal relaxation and diffusional contributions were achieved, where the efficient drug loading enables diffusional pathways and plastizing effects of chitosan, enabling chain mobility. Yet, at higher concentrations, aggregation of polyphenols blocks the pores, reducing the diffusion. Relaxational contribution persists because of the plastizing effect of the polyphenols. OH groups of the ellagic acid disrupt the H-bonding networks of chitosan, increasing the inter-chain volumes, while the COOH groups of gallic acid form complexes with NH_2 groups, decreasing the glass transition temperature of chitosan. These changes can be confirmed with the remaining higher k_R value and an increase in the m value due to pore occlusion in the matrix.

Balanced swelling and diffusion govern the release mechanism of the *SaC* composite in acidic media conditions with extreme swelling of the matrix. Partial protonation of NH_3^+ groups reduced k_D and k_R values at pH 2.5, compared to pH 1. At pH 4, the synergistic effects of swelling of chitosan and diffusion of weakly bound eugenol direct the optimal release conditions, creating porosity in the matrix (lower m value). Moderate k_D and k_R values were reported in physiological pH conditions, as a result of the partial collapse of the chitosan matrix in higher pH media. But the porosity remains due to eugenol's hydrophobic plastizising effects, preventing the complete compaction of chitosan chains during deprotonation. The increase in the k_D and k_R values at pH 10 suggests that the formation of stable pores in the matrix contributes to the prominent diffusional release, with the NaOH-induced partial hydrolysis of chitosan chains, resulting in diffusional pathways. k_D and k_R values are decreasing in the media ranging from 0.1–0.3 M as a result of the gradual increase of the masking of the charge in NH_3^+ groups, leading to shrinkage of the matrix. Diffusion is prominent in the swollen matrix, leading to the release of eugenol. However, at 0.4 M media, the partial collapse of the chitosan matrix induces transient pore formation along with matrix rearrangement. This phenomenon contributes to the synergistic effects of diffusion and relaxation. Complete charge screening is achieved at the highest ionic strength, resulting in the hydrophobic collapse of the matrix, forcing eugenol out of the matrix. Release pattern based on the drug concentration is consistent with *PeC* for *SaC* except for the fact that optimal synergistic effects were observed at 5 mg drug concentration with synergistic effects of relaxation and diffusion.

When categorised under the quasi-Fickian diffusion of the KP model, it does not distinguish the contribution of diffusion and relaxation mechanisms, but the PS model calculates these contributions. That can be observed by the values and the trends of the fluctuation of the k_R parameter in the PS model. Media with pH 7, 0.4 M NaCl and 7.5 drug concentration for *PeC* have indicated a sudden increment in the value of k_R corresponding to the increment in k_P, where the contributions of relaxation and diffusion were not taken into account separately. Further parameters of the PS model for *SaC* composite correspond with the n values obtained for the KP model, with higher diffusional release rate in media with pH 4, 0.1 M,0.2 M, 0.5 M and 5 mg drug concentration.

The model fits corresponding to the Higuchi model, Hixon-Crowell model, Zero order, and First order are represented in Figures S7–S10 (Chitosan: *P. emblica* composite) and Figures S14–S17 (Chitosan: *S. aromaticum* composite), respectively. Experimental cumulative drug release data were fitted with the Higuchi model, with higher R^2 values ($R2 \geq 0.96$) as shown in Tables S1-S6, along with the other model parameters. Although conceptually simple, the Higuchi model depends on several fundamental presumptions in order to adequately represent controlled drug release systems. First, it assumes that the starting drug concentration is much more than the drug's solubility, which supports the application of a pseudo-steady-state method. Second, the model assumes that drug diffusion occurs in one dimension, which makes edge effects insignificant. Third, it assumes that the drug particles in suspension(micro or nano) are significantly smaller than the thickness of the system. Furthermore, the model assumes a steady drug diffusion coefficient, ignoring any swelling or relaxation of the polymer carrier[117]. Together, these presumptions support the model's applicability and constraints in forecasting drug release behavior. Optimal release rates for the *PeC* are recorded in the media with pH 1 and 0.2 M NaCl, where the swelling of the chitosan enhances the diffusion. A slight increase in the k_H in media with pH 10 for *PeC* is attributed to the increased diffusion rates with the NaOH-induced pore formation. For the *SaC* composite, release conditions are optimal in the media with pH 4, and the release rates are consistent in neutral media as well. Interestingly, when the drug concentration was increased, the release rate was shown to be increased according to the K_H values reported in Table 5, supporting the model assumption. Although it is believed that the correlation between the cumulative drug release and the square of time is a valid metric for examining

drug release in a diffusion-controlled drug delivery system (Eq. 9), it is possible to get incorrect conclusions about the drug delivery mechanism if this model is used exclusively for analysis. Because it entirely ignores the swelling or dissolution effect of the polymeric carrier system in its primary assumption[118]. Therefore, additional mathematical studies are necessary to determine the drug release mechanism if the Higuchi model is used.

The drug release is predicated on the idea that a solid particle's surface area reduces as it dissolves. According to the Hixon-Crowell model (HC). The surface area reduction is proportional to the cube root of the particle's residual mass[119]. The approach works especially well in conditions where the dissolving particle undergoes significant size and shape changes, such as a tablet in a fluid. In these situations, when the drug is released, the tablet's surface area steadily decreases[120]. Nevertheless, since the release of the bioactive compounds was shown to be dependent on diffusion and relaxation, rather than constant reduction of the surface area of the polymer HC model is not used in the current study to interpret the controlled release. This is further concluded by the lower R^2 values obtained for the fitted drug release data of the synthesized drug composites.

The fundamental premise of the zero-order kinetics model is that the rate of reaction is completely independent of the concentration of the reactant, meaning that a fixed quantity of reactant is used up per unit of time[121]. On the other hand, the first-order kinetics model assumes that the reactant concentration and reaction rate are exactly proportional. In first-order kinetics, the rate fluctuates with changes in concentration, but in zero-order kinetics, the rate is essentially constant regardless of concentration. Additionally, in situations where $n = 1$, the first order is theoretically equivalent to the KP model, suggesting that the case II transport mechanism is the cause of the drug release[122]. R^2 for the Zero and First order models in the fitted release data are less than 0.95 in all the media compositions reported for *PeC* and *SaC* drug composites. Therefore, these mechanisms were not the only governing factor that was responsible for the release of bioactive compounds.

In conclusion, non-linear curve fitting data attributed to the in vitro study suggest that a combination of diffusion and polymer relaxation mechanisms controls the release of ellagic acid, gallic acid, and eugenol, present in the plant extracts of *P. emblica* and *S. aromaticum*, from chitosan biopolymer over time. The work demonstrates how release mechanisms are dependent on pH and ionic strength, with hydrophobic partitioning driving *SaC* and swelling/polyphenol solubility driving *PeC*. The KP and PS models verified diffusion-dominated release with relaxing effects under particular conditions, ensuring the sustained release of bioactive compounds. Therefore, the sustained release of the targeted bioactive compounds was achieved using the chitosan-based delivery system, improving the pharmacokinetic parameters of the potential therapeutic agents.

Antibacterial activity by agar well diffusion method

Antibacterial activity

Samples consisting of different ratios of chitosan and CuO were synthesized as follows: Chi, CuO, Chi:CuO 1:1, Chi:CuO 1:2, Chi:CuO 1:3, Chi:CuO 1:4, Chi:CuO 2:1, Chi:CuO 3:1 and Chi:CuO 4:1. And to these nanocomposites the tested plant extracts were coated by mixing and evaporating the solvent to evaluate the synergistic impact of the plant materials; *Phyllanthus emblica*, and *Syzygium aromaticum* along with chitosan and CuO.

Chitosan, a multifaceted hydrophilic polysaccharide derived from chitin, has a wide antibacterial spectrum, rendering it particularly effective against gram-negative and gram positive bacteria as well as fungi[123–127]. Its efficacy is influenced by factors such as molecular weight, degree of deacetylation, and environmental pH[128]. The mechanisms of the antibacterial activity of chitosan towards pathogenic bacterial species are varied. At the site of infection, chitosan can form a film that acts as a barrier, hindering nutrient uptake by bacteria and effectively starving them. The polycationic nature of chitosan enables it to interact with the negatively charged bacterial cell membranes, leading to increased permeability and subsequent leakage of intracellular contents, culminating in cell death[129]. Chitosan can chelate essential metal ions, thereby inhibiting bacterial enzyme activities and disrupting metabolic processes[124,130]. Additionally, the degree of deacetylation (DDA) significantly influences chitosan's antibacterial properties. Higher DDA correlates with increased positive charge density, enhancing interactions with bacterial membranes and improving antimicrobial efficacy[124]. Environmental pH also plays a crucial role; chitosan exhibits increased solubility and antimicrobial activity in acidic conditions due to the protonation of its amino groups, facilitating stronger interactions with bacterial cells. Studies have demonstrated chitosan's effectiveness against both Gram-positive and Gram-negative bacteria. For instance, chitosan nanoparticles have shown enhanced antimicrobial activity against a range of pathogenic bacteria, including *Escherichia coli* and *Staphylococcus aureus*[128,129,131].

Multiple articles investigated the antibacterial properties of elemental Cu, CuO, and Cu_2O, addressing factors such as particle size, shape, and the solubility of copper ions in various media. The antibacterial effect of CuO is associated with a rapid deterioration of cell membrane integrity and the generation of reactive oxygen species (ROS)[30] However, the difference in cell wall structures of Gram-negative and Gram-positive bacteria, as depicted in Fig. 11, determines the overall antibacterial activity of nanomaterials. Moreover, chemical doping with other components has amplified the antibacterial range and diminished the necessary dose for pathogen suppression. These results jointly emphasize the significance of chemically synthesized CuO nanomaterials as effective antibacterial agents in clinical and industrial contexts[132–135]. Moreover, its cost and availability are more favourable than silver, gold, and platinum metals. Copper has historically served as an antibacterial agent due to its low toxicity and is important in the biomedical field[134–136]. Owing to their diminutive size relative to bacterial pores, these nanomaterials possess a distinctive capability to infiltrate the cell membrane, as shown by CuO nanomaterials. The band gap of CuO is around 1.7 eV, and this kind exhibits semiconductor characteristics in a non-crystalline structure[132,137] .

Copper oxide has significant antibacterial properties via several methods, rendering them efficient against many bacterial infections as shown in Fig. 12. It is assumed that materials containing CuO nanomaterials are capable of killing both Gram-positive and Gram-negative bacteria through the "attract-kill-release" pathway[138].

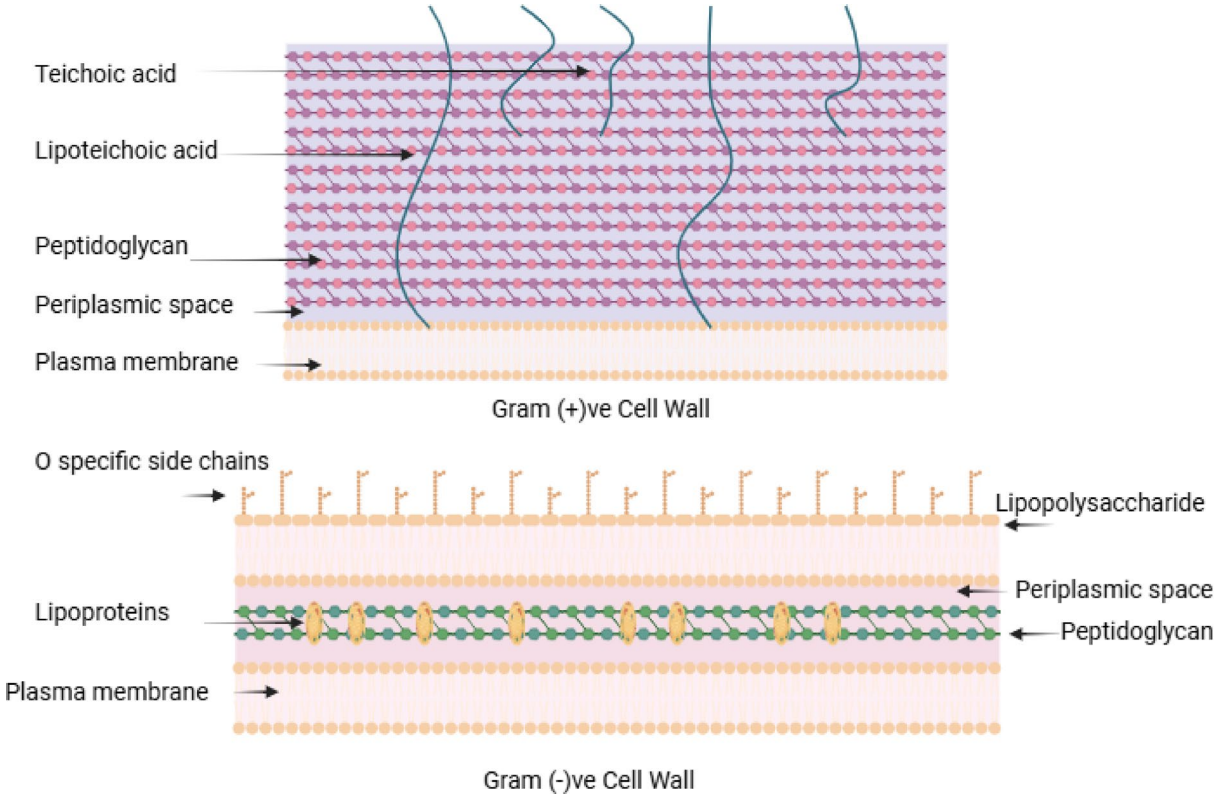

Fig. 11. The cell wall structures of gram-negative and gram-positive bacteria.

Reactive oxygen species generation and the release of Cu^{+} ions from CuO nanomaterials are both thought to be responsible for the contact killing of bacteria[133,138]. The inherent characteristics of CuO, such as its monoclinic crystalline structure and elevated surface-to-volume ratio, facilitate the effective rupture of bacterial cell walls via the formation of ROS and membrane degradation[133,139–143]. Furthermore, nanorods are hierarchical CuO nanostructures showing significant antibacterial activity[143]. Another significant mechanism involves the liberation of copper ions ($Cu2^{+}$) from the CuO nanomaterials, which engage with thiol groups in bacterial enzymes, therefore impairing vital metabolic processes. These ions disrupt DNA replication by binding to nucleic acids, hence reducing bacterial multiplication[144].

Advanced research on chitosan nanoparticles (CsNPs) has shown improved antibacterial efficacy, which is attributed to their increased surface area and bioavailability, facilitating superior contact with bacterial cells. CsNPs affect outer membrane production, metabolic processes, and membrane signalling, as shown by transcriptome analysis in *Escherichia coli*[145]. The predominant mechanism of CsNPs' antibacterial activity is the electrostatic interaction between the positively charged amino groups of glucosamine and the negatively charged bacterial cell membranes[146]. This interaction causes significant alterations to the cell surface, resulting in changes in membrane permeability that subsequently provoke osmotic imbalance and the outflow of intracellular chemicals, culminating in cell death[147,148].

Microbes' resistance to most antibiotics typically used for infections (including penicillins, cephalosporins, erythromycin, tetracycline and its derivatives, and metronidazole) has been recorded. The resistance of bacteria to conventional antibiotics necessitates an immediate focus on the advancement of novel medication compounds. Historical records indicate that phytochemicals have been used as remedies for several ailments and microbiological illnesses since ancient times.

Therefore, the amalgamation of chitosan with CuO and plant extracts can produce nanocomposites with significant antibacterial efficacy, presenting intriguing applications in combating microbial diseases and fabricating antimicrobial materials.

Various nanocomposites, synthesized by combining CuO and Chitosan in different ratios, were evaluated against all four harmful bacteria. The data shown in Fig. 13a clearly indicate that the various samples had distinct effects on all four tested bacteria; *Klebsiella pneumoniae, Pseudomonas aeruginosa, Escherichia coli* and *Staphylococcus aureus*. At the lowest concentration tested at 10 mg/ ml, the highest zone of inhibition was recorded for *Klebsiella pneumoniae* at 11.83 ± 3.21 mm across all samples tested, indicating low resistance potential against the novel nano-biocomposites. Moderate zones of inhibition were recorded for *Pseudomonas aeruginosa* and *Escherichia coli*, ranging from 8.00 ± 0.29 to 10.83 ± 1.53 mm across all samples. The resistance levels of the pathogens against the synthesized materials may be substantiated by analyzing their structural properties and resistance mechanisms. *Klebsiella pneumoniae*, has a more intricate outer membrane and demonstrates enhanced biofilm formation, which contributes to its increased resistance[149]. They also possess

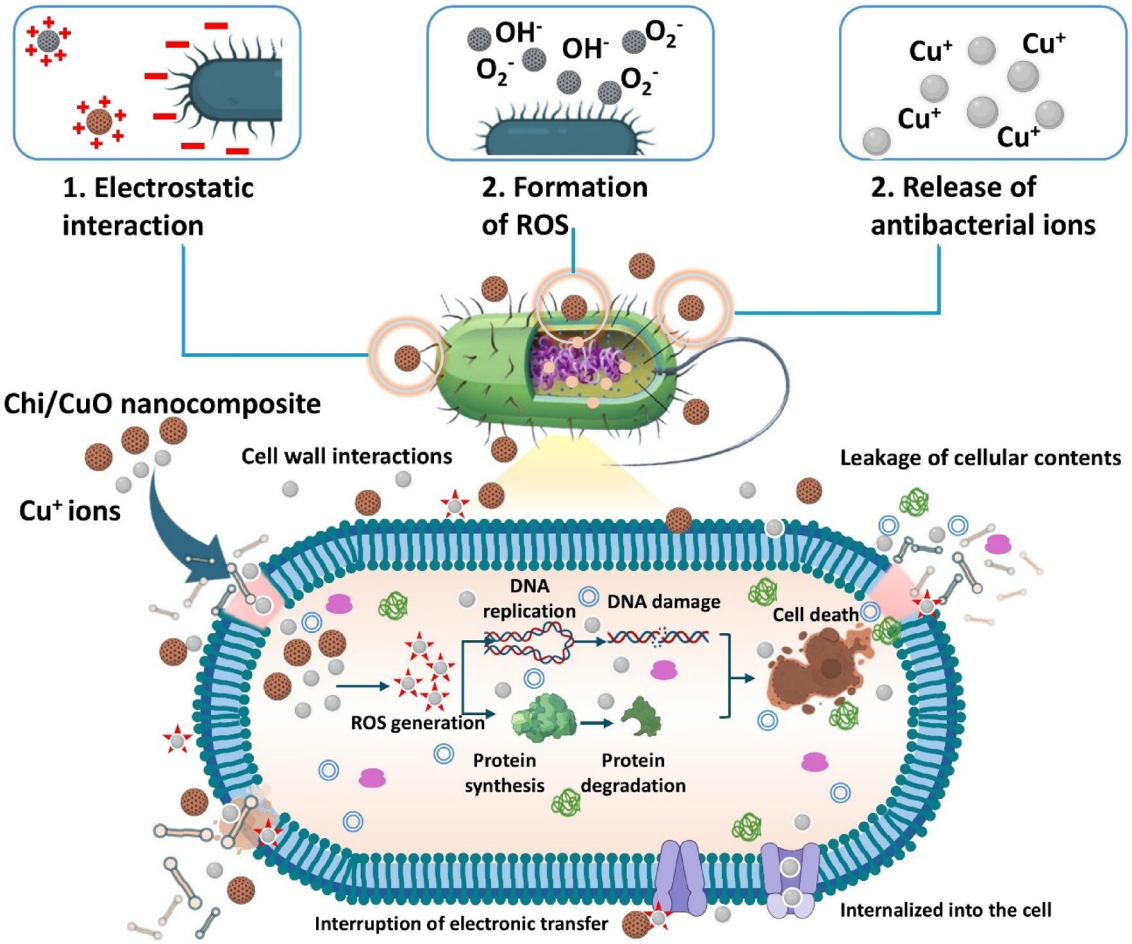

Fig. 12. Mechanisms of the antibacterial activity of Chi:CuO nanocomposites.

a protective outer membrane and polysaccharide capsule, hindering particle penetration[150]. They demonstrate several resistance mechanisms, such as efflux pumps and biofilm formation, which markedly diminish the effectiveness of nanoparticles[149]. Furthermore, Cu^{+} may provoke oxidative stress in bacteria, yet *Klebsiella*'s adaptive mechanisms can alleviate this impact[151]. However, the concentration of nanoparticles are critical to their efficacy against various bacterial strains[149]. Research suggests that chitosan nanoparticles enhance the bioavailability of antibiotics, possibly resulting in decreased dosage requirements and diminished resistance development, although the existence of many antibacterial mechanisms as mentioned above[152].

In terms of Gram-positive bacteria, *Staphylococcus aureus* has not shown significant resistance against the nanocomposites with zones of inhibition ranging from 8.67 ± 1.44 to 10.17 ± 0.29 mm. *Staphylococcus aureus*, especially methicillin-resistant strains (MRSA), has a certain vulnerability to nanocomposites owing to its comparatively more uncomplicated cell wall structure, facilitating efficient particle penetration[153]. Moreover, *Staphylococcus aureus* has a thick peptidoglycan layer that may be targeted by the produced ions. Nanomaterials may inhibit biofilm development, increasing treatment susceptibility[153]. Chitosan:CuO 1:2 was shown to be the most efficient against all pathogenic strains, effectively reducing bacterial growth and suggesting optimal efficacy at low concentrations.

Different nanocomposites prepared by integrating CuO and Chitosan in different ratios were tested against all four pathogenic microorganisms. From the results given in Fig. 13b, it is evident that different samples have acted differently on all four microorganisms. Against *Klebsiella pneumoniae* sample Chi:CuO 1:4 has been most effective in inhibiting the growth by showing a zone of inhibition of 16.50 ± 0.09 mm while Chi:CuO 1:3 has been most effective on *Pseudomonas aeruginosa* with a zone of inhibition of 12.67 ± 0.20 mm. For *E. Coli* the Chi:CuO 1:2 sample has shown the most significant inhibition with a zone of inhibition at 11.83 ± 0.06 mm. For the Gram-positive *Staphylococcus aureus*, Chi:CuO 1:4 has been most efficient with a zone of inhibition of 12.92 ± 0.06 mm. The stronger resistance shown by Gram-negative bacteria could be due to the architecture of their cell membranes. The outer membrane of Gram-negative bacteria, which contains lipopolysaccharides that serve as an additional protective film, can hinder the penetration of the antibacterial compounds, limiting the overall sensitivity against the samples[154,155]. They also contain an increased number of efflux pumps that have the ability to expel the antibacterial compounds from the bacterial cells, limiting the interactions of these with

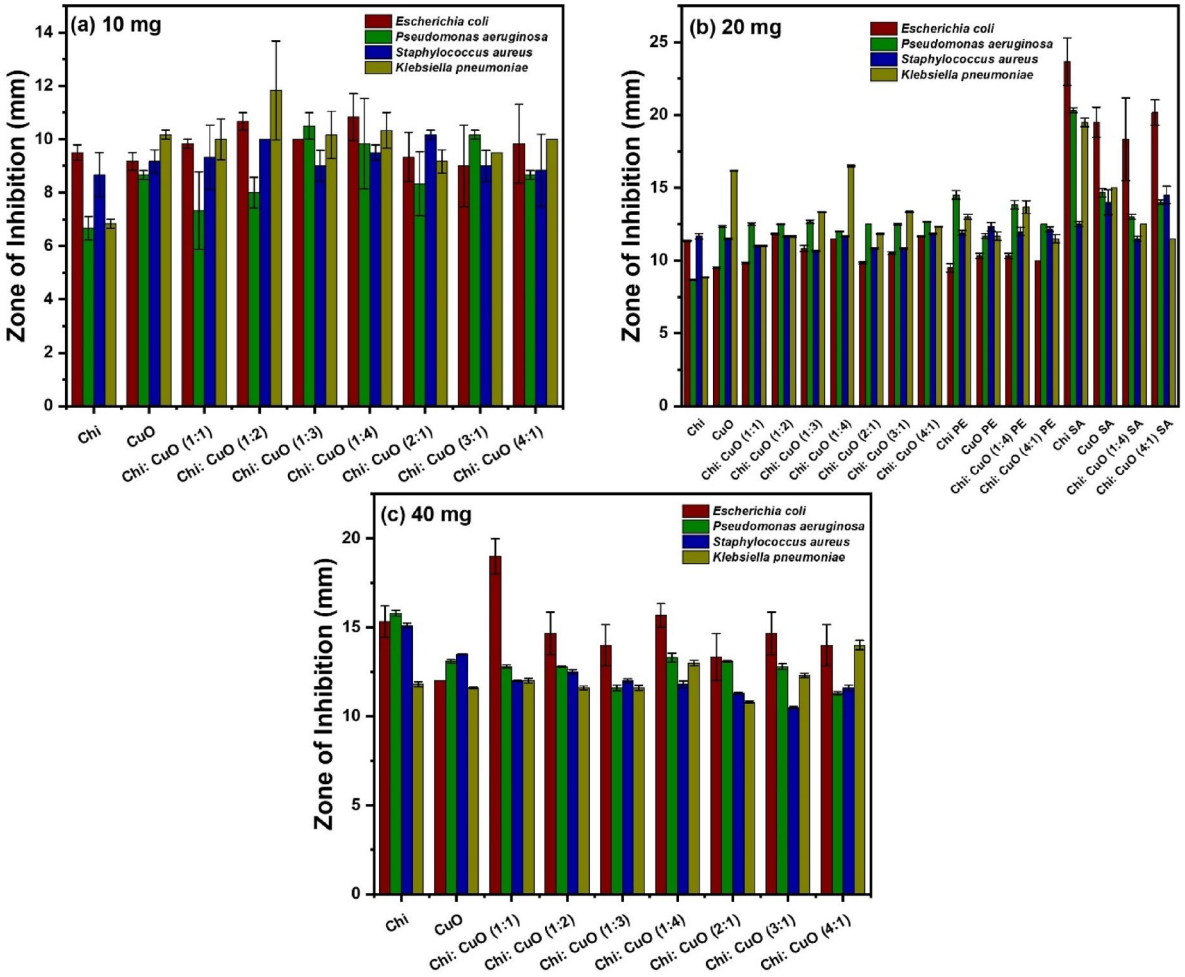

Fig. 13. Antibacterial activity of synthesized Chi:CuO nanocomposites and *P. emblica*, *S.aromaticum* coated composites at (**a**)10 mg/ml (**b**) 20 mg/ml and (**c**) 40 mg/ml.

the intracellular components[156]. Additionally, Gram-negative bacteria have the ability to alter efflux pumps and porins, which can affect the uptake and expulsion of antibacterial compounds from the cell[157].

The antibacterial activity of the nanocomposites Chi, CuO, Chi:CuO 1:1, Chi:CuO 1:2, Chi:CuO 1:3, Chi:CuO 1:4, Chi:CuO 2:1, Chi:CuO 3:1 and Chi:CuO 4:1 are presented in Fig. 13c at 40 mg/ ml. The overall antibacterial activity of the samples has increased with the increased concentration from 10 to 40 mg/ ml. Across samples, the lowest zone of inhibition recorded was 10.10 ± 0.03 mm against *E. Coli* from Chitosan:CuO 4:1, while the highest zone of inhibition was recorded at 15.80 ± 0.30 mm against *Pseudomonas aeruginosa* from Chitosan. Interestingly, Chitosan has shown the overall highest antibacterial activity against *Klebsiella pneumoniae, Pseudomonas aeruginosa, Escherichia coli* and *Staphylococcus aureus*. Even though it was assumed that incorporating CuO, a well-known antibacterial compound, would increase the inhibition potential against pathogens, it has not shown the expected synergistic effects with chitosan, at the tested concentration. Similarly, in Chitosan, CuO, Chi:CuO 1:1, Chi:CuO 1:2 to Chi:CuO 1:3, the overall antibacterial activity has decreased. CuO at elevated concentrations seems to have little influence on antibacterial activity. The Chi: CuO 4:1 sample had the lowest antibacterial efficacy against all tested strains, including *Klebsiella pneumoniae*, *Pseudomonas aeruginosa*, *Escherichia coli*, and *Staphylococcus* at the tested concentrations.

The morphological alterations resulting from the elevated concentration of the synthesized nano -biocomposite are presumed to influence antibacterial activity owing to their bulky characteristics. Previous research demonstrates that CuO-NP has diminished antibacterial efficacy at higher concentrations, commencing at 26.5 µg/ml, owing to concentration-induced aggregation, which modifies *S. aureus* sensitivity, as seen by the biphasic dose–response noted in a microbial viability experiment[158]. Another study demonstrated that CuO had superior antibacterial activity compared to ZnO, with minimum inhibitory concentrations of 1 mg/ml for *E. coli* and 0.25 mg/ml for *S. aureus*, indicating that increased concentrations may not improve performance owing to saturation effects[159]. CuO has also exhibited lower antibacterial action at higher concentrations owing to variations in size, shape, aggregation, and settling behaviour of bulk particles, resulting in reduced biofilm inhibition[160]. Therefore, these findings highlight that while CuO exhibits substantial antibacterial properties,

excessive concentrations may hinder its effectiveness due to aggregation and saturation effects. Optimizing concentration levels is crucial for maintaining its antibacterial efficacy.

To assess the synergistic impact of Chitosan-CuO nanocomposites with herbal extracts, the most effective biocomposites and the optimal concentration 20 mg/ ml, determined by the overall highest zone of inhibition, were selected for combination with *Phyllanthus emblica* (Indian gooseberry,), and *Syzygium aromaticum* (Clove). Consequently, the selected samples, Chi, CuO, Chi:CuO 1:4, and Chi:CuO 4:1, were combined with herbal extracts. The obtained results are given in Fig. 13b, while the inhibition zones obtained from the well diffusion method are depicted in Fig. 14. Among the best four performing samples tested Chi, CuO, Chitosan:CuO 1:4, and Chitosan:CuO 4:1, the clove-loaded chitosan sample exhibited the highest zone of inhibition against *Klebsiella pneumoniae*, measuring 19.50 ± 0.50 mm. In contrast to previous discoveries that did not employ herbal extract coating, CuO has shown no significant effect on the antibacterial activity against *Klebsiella pneumoniae*, however clove has been crucial in inhibiting and reducing the proliferation of this specific microorganism. The maximum zone of inhibition for *Pseudomonas aeruginosa* was 20.33 ± 0.29 mm, whereas for *Escherichia coli* it was 23.67 ± 2.84 mm, both achieved using the same biocomposite, clove-loaded chitosan. Conversely, the gram-positive *Staphylococcus aureus* exhibited the highest inhibition at 14.50 ± 1.04 mm due to clove loading with Chitosan:CuO 4:1. Chi:CuO 4:1 has demonstrated a significant impact on the synergistic interaction among chitosan, CuO, and clove extract. The amalgamation of chitosan with CuO and clove extract has previously also resulted in enhanced antibacterial activity, as each constituent addresses distinct antibacterial mechanisms. Chitosan improves the solubility and stability of CuO, whilst clove extract offers supplementary antibacterial properties[161,162]. Research demonstrates that the combination of chitosan and clove extract is very potent against Gram-positive bacteria, hence increasing the overall antibacterial effectiveness of food coatings[163].

Among herbal extracts, clove had the most significant antibacterial activity against all four tested pathogens. Indian gooseberry has significant antibacterial action, inferior to that of clove. The rationale for this is likely the antibacterial properties of the primary bioactive components in these extracts, in conjunction with the synergistic effects of chitosan and CuO. CuO nanorods are immobilized on the chitosan matrix. These nano rods can easily perforate the bacterial cell wall and the membrane and hence easily penetrate the microorganism due to its sharp edges as shown in the Fig. 15. The intracellular material will be leaked due to the holes created through perforation and penetration of the nanorods, eventually leading to cell death.

Clove extracts have significant antibacterial activity, principally due to their abundant phytochemical constituents, such as eugenol, phenolics, flavonoids, and tannins. These chemicals compromise bacterial cell structures and obstruct vital biological processes, making clove extracts effective against several bacterial strains. Eugenol, a principal constituent of clove essential oil, compromises the structural integrity of bacterial cell walls and membranes, particularly in *Staphylococcus aureus*, resulting in the efflux of intracellular materials and subsequent cell death[164]. Scanning Electron Microscopy (SEM) has shown that clove extract may modify the shape of *Vibrio alginolyticus* cells, suggesting physical damage to bacterial structures[165]. Clove extracts disrupt biofilm formation, essential for bacterial survival and resistance. Eugenol diminishes biofilm cellular activity in both *S. aureus* and *Escherichia coli*, thereby impeding their development. Eugenol treatment enhances the generation of ROS in bacterial cells, resulting in oxidative stress and death. This is followed by increased activity of antioxidant enzymes, which ultimately surpasses the bacterial defense systems[164]. Clove extracts have shown promise in augmenting the effectiveness of antibiotics against multidrug-resistant bacteria. Despite the absence of direct contact, the amalgamation of clove extract with antibiotics such as nitrofurantoin and ciprofloxacin decreased the minimum inhibitory concentrations of these agents[166]. Similarly, the incorporation of chitosan and CuO must have contributed to the substantial antibacterial activity of the composite.

The antibacterial action of *Phyllanthus emblica* (Indian gooseberry) extracts is mainly due to its abundant phytochemical constituents, including phenolics, flavonoids, and tannins. *P. emblica* has elevated concentrations of phenolics and flavonoids, recognized for their antioxidant and antibacterial characteristics[167]. Analysis indicates the existence of carboxyl, carbonyl, and aromatic groups, which enhance its antibacterial effectiveness[168]. Molecular docking studies reveal that substances such as sitosterol have significant antibiofilm efficacy by inhibiting bacterial adhesion and proliferation[169] The antioxidant ability of *P. emblica* extracts may contribute

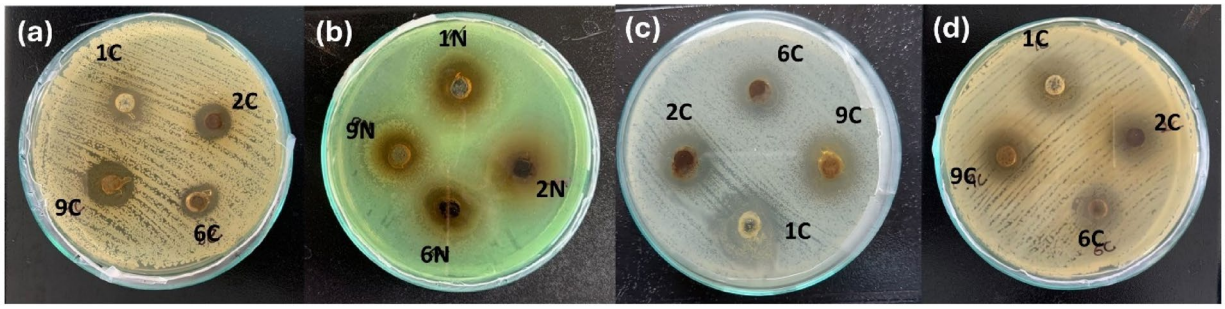

Fig. 14. Antibacterial activity of synthesized plant extract coated composites (20 mg/ml) with test organisms. (**a**) *Staphylococcus aureus* (**b**) *Pseudomonas aeruginosa* (**c**) *Escherichia coli* and (**d**) *Klebsiella pneumoniae*.. 1–Chitosan, 2–CuO, 6–Chi:CuO (1:4), 9–Chi:CuO (4:1) and N–*Phylanthus emblica* extract, C–*Syzygium aromaticum* extract.

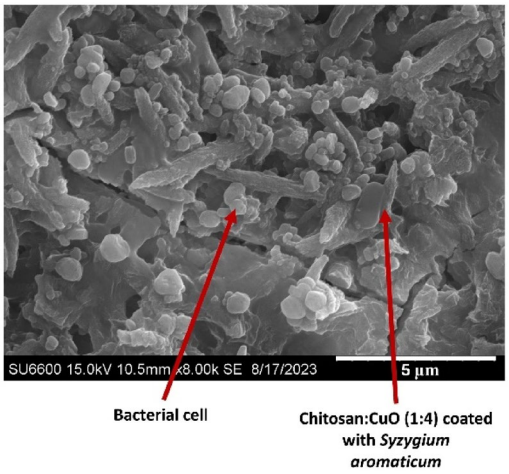

Fig. 15. SEM image of antibacterial mechanism of Chi:CuO (1:4) nanocomposite coated with *S. aromaticum* extract.

Pathogen	MIC (mg/mL)		MBC (mg/mL)	
	Chi: CuO (1:4)PE	*Chi SA*	*Chi: CuO (1:4)PE*	*Chi SA*
Klebsiella pneumoniae	2.50	10.00	0.63	40.00
Pseudomonas aeruginosa	0.31	0.31	0.31	0.31
Escherichia coli	0.31	0.31	0.31	0.31
Staphylococcus aureus	0.31	2.50	0.31	40.00

Table 6. MIC and MBC activity of the tested composites.

to reducing oxidative stress in bacterial cells, hence augmenting their antibacterial actions[167]. The antibacterial action is shown to be dose-dependent, with increased concentrations resulting in enhanced inhibition[169].

The positive control, Amoxicillin, showed higher zones of inhibition than the *P. emblica* extract and the nanocomposites against all test microorganisms at 10, 20, and 40 mg/mL, but *S. aromaticum* extract exhibited a higher inhibition zone than the positive control against all the tested microbial species at all three concentrations. The highest zone of inhibition for Amoxicillin was recorded against *Escherichia coli* with a zone of 40.0 ± 0.67 mm at 40 mg/ mL.

In conclusion, clove and Indian gooseberry extracts have exhibited significant antibacterial potential through diverse mechanisms, making them promising candidates for antimicrobial applications. Clove's efficacy is primarily attributed to eugenol, which disrupts bacterial cell membranes and inhibits enzyme activity. Indian gooseberry, abundant in polyphenols enhances oxidative damage and disrupts microbial biofilm formation[164,165,168–171]. The synergistic action of these natural extracts with biomaterials like chitosan and metal oxides like CuO has further enhanced their antibacterial properties, offering a sustainable and effective alternative for biomedical, food preservation, and pharmaceutical applications.

MIC and MBC assay The MIC and MBC values were determined for all four test microorganisms. MIC is the minimum concentration of a substance that can prevent the observable growth of an organism, while MBC is the minimum concentration that inhibits growth in batch cultures. This can be ascertained from broth dilution MIC tests by subculturing onto agar media devoid of antibiotics[162,172,173]. The determined MIC, MBC, and MBC/MIC values are shown in Table 6.

The antibacterial activity was further evaluated based on the MBC/MIC ratio. If the MBC/MIC ratio ≤ 4, the effect is bactericidal, and if the MBC/MIC > 4, the effect is bacteriostatic[172]. Out of the samples coated with Clove, and Indian gooseberry tested, the best-performing samples from each category, depending on the overall antibacterial activity, were chosen for further evaluation. Therefore, Chi:CuO 1:4 coated with Indian gooseberry extract, and chitosan-coated with clove extract were chosen for the MIC/ MBC assay. The selected samples were tested against, *Klebsiella pneumoniae, Pseudomonas aeruginosa, Escherichia coli* and *Staphylococcus aureus* to derive MBC/ MIC values. The Chitosan sample coated with clove extract demonstrated an MBC/MIC ratio of 16 against *Staphylococcus aureus*, while the other samples; Chi:CuO 1:4 coated with Indian gooseberry extract against *Klebsiella pneumoniae*, *Pseudomonas aeruginosa*, *Escherichia coli*, and *Staphylococcus aureus*, showed MBC/MIC values of 4 or lower. In particular, the Chitosan sample coated with clove extract exhibited MBC/ MIC values of 4 or below against all tested pathogens except for *Staphylococcus aureus*. Consequently, it may be inferred that only the Chitosan sample coated with clove extract exhibits bacteriostatic properties, whereas all other samples demonstrate bactericidal effects.

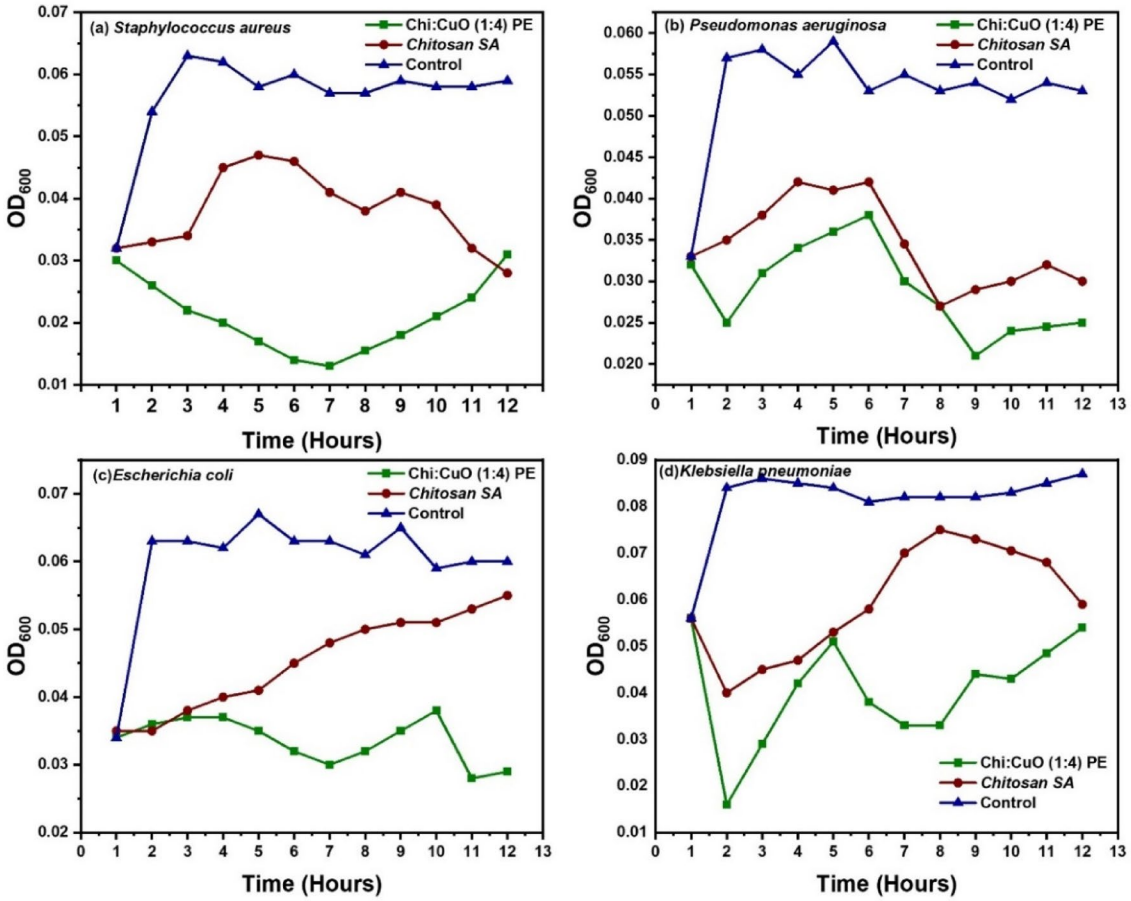

Fig. 16. Time-kill curves of the test organisms (**a**) *Staphylococcus aureus* (**b**) *Pseudomonas aeruginosa* (**c**) *Escherichia coli* and (**d**) *Klebsiella pneumoniae*.

The assertion about the MBC/MIC ratio as a factor influencing bactericidal vs. bacteriostatic effects is based on pharmacodynamics. The Minimum Bactericidal Concentration (MBC) is the minimal concentration of an antibiotic that eradicates a particular bacteria, while the Minimum Inhibitory Concentration (MIC) is the minimal concentration that suppresses its growth[172,174]. In clinical environments, comprehending this ratio facilitates the selection of suitable antibiotics, especially for resistant bacteria, hence assuring successful treatment results. A ratio of < 4 often indicates that the medicine successfully eradicates germs, as shown by vancomycin against certain strains of *Staphylococcus aureus*, where lower ratios corresponded with substantial bacterial decrease[174]. Discrepancies in MBC and MIC values across bacterial strains might result in varying treatment effects. Tolerant strains may have elevated MBC values despite low MICs and confounding treatment considerations[175]. Bactericidal agents, such as cephalosporins and other beta-lactam antibiotics, obstruct the synthesis of bacterial cell walls. Bacteriostatic drugs, such as chloramphenicol and clindamycin, inhibit or retard bacterial proliferation by obstructing protein synthesis[172,173,176]. The MIC and MBC tests supply essential information on an antibacterial agent's mechanism of action.

Time-kill synergy assay The antibacterial efficacy of the composites was then assessed in a liquid media by conducting a time-kill synergy testing on the tested bacteria. The concentration of materials (20 mg/ml) exhibited substantial antibacterial activity against gram-negative *Escherichia coli*, *Pseudomonas aeruginosa*, and *Klebsiella pneumoniae*. Gram-positive *Staphylococcus aureus* was similarly inhibited at doses of 20 mg/ml. Figure 16 illustrates the time-kill curves generated for the investigated bacterial pathogens in relation to all the studied composites. Bacterial suspensions in LB broth underwent a 12-h time-kill kinetic test with the incorporation of composites (20 mg/ml), and observations were recorded at 600 nm. The time-kill curve of composites against all examined bacterial pathogen strains exhibited a time-dependent firm inhibitory effect, which immediately impacted the bacterial cells prior to their attainment of the stationary phase. The growth curves of bacteria subjected to composites indicate that these substances may impede both bacterial proliferation and reproduction. We have shown that synthesized materials can impede the proliferation of Gram-negative and Gram-positive bacteria by MIC tests, MBC tests, and traditional growth curves. The growth and development of all the tested bacterial strains were obstructed by the tested composites; Chi: CuO(1:4) coated with *P. emblica* and chitosan coated with *S. aromaticum* during the lag or log phase.

A feature intrinsic to microbial kinetics is lag, often characterized as a delayed reaction of the microbial population to an abrupt environmental change. A lag phase may manifest in both growth and inactivation processes. Under favourable growth circumstances, the lag phase serves as an adaptation stage during which bacterial cells alter their physiology to exploit the new environment and commence exponential development[177]. This phase is marked by metabolic modifications, alterations in gene expression, and the buildup of vital nutrients. The duration of the lag phase may vary, often ranging from minutes to hours, depending upon the species and environmental factors. In contrast, in the log phase is characterized by accelerated cellular proliferation and population growth. In this phase, bacteria proliferate at a steady and maximum pace, resulting in a predictable population doubling time. This phase is essential for comprehending bacterial dynamics in many habitats, as it indicates ideal growth circumstances[172,178]. It is essential to recognize that not all bacterial populations have consistent growth patterns owing to environmental heterogeneity, perhaps resulting in prolonged lag periods or early shifts to stationary phases[179]. The related euations are mentioned in the supplementary information (**Eqs.** 1–3).

The antibacterial properties of clove, Indian gooseberry, chitosan, and CuO operate via many mechanisms that compromise bacterial cell integrity and functionality. Each agent utilizes specific mechanisms to exert its effects, including the inhibition of bacterial enzyme activity and the disruption of cell wall synthesis, resulting in cell lysis; the disruption of cell membranes, causing leakage of intracellular components; and the elevation of oxidative stress, ultimately inducing cell apoptosis. Additionally, the generation of ROS damages bacterial cell membranes and DNA, culminating in cell death[123,124,133,135,163–166,170–172,180–182]. Eventually, the size of a bacterial cell suitable for a certain environmental context and developmental outcome is attained by coordinating cell growth and division. When such synchronization is interrupted, the developmental trajectory is affected[172,183] therefore exhibiting deviations from a normal bacterial growth curve.ss

Conclusion

Chitosan, a naturally derived biopolymer was synthesized using shrimp shell waste material and it was hydrothermally coupled with CuO nanoparticles at nine ratios to synthesize the nanocomposite materials used in the study. Further, the nanocomposites were coated with the *Phyllanthus emblica* and *Syzygium aromaticum* methanolic plant extracts to synthesize the coated nanocomposites. Antioxidant, anti-inflammatory, and antibacterial activities as well as the total phenolic content and phytochemical analysis of the plant extracts and developed composite materials were tested. According to the 2,2-diphenyl-1-picrylhydrazyl assay, the antioxidant activity of the *Phyllanthus emblica* coated chitosan composite varied from 45.36% (0.005 mg/mL) to 94.88% (0.025 mg/mL), and the antioxidant activity of the *Syzygium aromaticum* coated chitosan composite varied from 19.75% (0.005 mg/mL) to 58.98% (0.025 mg/mL). Considering the egg albumin denaturation assay, the anti-inflammatory activity of *Phyllanthus emblica* coated chitosan composite varied from 13.98% (0.1 mg/mL) to 74.30% (0.7 mg/mL), and the anti-inflammatory activity of *Syzygium aromaticum* coated chitosan composite varied from 21.98% (0.1 mg/mL) to 80.00% (0.7 mg/ml). The total phenolic content of all the samples tested varied in the range of 45.43–45.78 mg GAE/mL. In the antibacterial study, Chitosan: CuO 1:4 was shown to be the most efficient against all pathogenic strains, effectively reducing bacterial growth and suggesting optimal efficacy, and out of the coated samples, *SaC* was the most effective against all tested organisms at 20 mg/mL. The tested composites obstructed the growth and development of all the tested bacterial strains (Chi: CuO 1:4) PE, (Chi) SA at the lag or log phase, as shown in the time-synergy kill curve. Plant extract-coated chitosan composites were tested for their potential to be used as a controlled delivery system by enhancing the pharmacokinetic properties of bioactive compounds, including gallic acid, ellagic acid, and eugenol. According to the drug delivery study results, Quasi-Fickian diffusion was proven to be the responsible release mechanism of the bioactive compounds from the chitosan delivery system. This investigation showed that the release of *PeC* and *SaC* composites was dependent on both pH and ionic strength. The protonation of NH_2 groups caused swelling increasing the release while deprotonation (pH > 6.7) caused the collapse reducing the diffusion. Further, the porosity of the polymer matrix was changed with Na^+ and Cl^- ion concentration as they shielded the NH_3^+ groups. As shown in the study, the hydrophobic nature of eugenol, the formation of H-bondings by the phenolic and carboxylic groups in ellagic acid and gallic acid and weaker van der Waals interactions of eugenol were the key factors governing the release of bioactive compounds from the chitosan matrix. Because of chitosan swelling and polyphenol solubility, *PeC* exhibited burst release at pH 1, whereas release declined at neutral-alkaline pH as the matrix collapsed due to the deprotonation of NH_3^+ groups. *SaC* showed improved release at high ionic strength (0.4–0.5 M NaCl) and optimal release at pH 4 mediated by hydrophobic interactions. Release kinetics analysis showed that both systems were dominated by quasi-Fickian diffusion, with *SaC* favoring hydrophobic expulsion and *PeC* being responsive to ionic shielding. Both composites demonstrated their potential for controlled drug release at physiological conditions (pH 7.4, 0.2 M NaCl) by achieving sustained release, with *SaC* via hydrophobic nanochannels and *PeC* through residual porosity. Therefore, diffusion supported by the relaxation and swelling of the polymer network is responsible for the release of the bioactive compounds. This study has several limitations, including the absence of in vivo experiments, the restricted water solubility of the delivery system attributed to the high molecular weight of chitosan, and the lack of cytotoxicity, metabolic, and excretion assays, as well as evaluations of potential cumulative effects that could impact drug safety. Consequently, additional in vivo studies are necessary to investigate the antioxidant and anti-inflammatory properties and the efficiency of drug delivery. Moreover, the potential of chitosan as a carrier molecule for the targeted delivery of the bioactive compounds gallic acid, ellagic acid, and eugenol to specific tissues requires thorough investigation. Further research should focus on assessing the cytotoxicity and safety profile of the newly synthesized drug composite to ensure its therapeutic applicability.

Data availability

The datasets used and/or analyzed during the current study are available from the corresponding author on reasonable request.

Received: 13 March 2025; Accepted: 11 September 2025
Published online: 13 October 2025

References

1. Adepu, S. & Ramakrishna, S. Controlled drug delivery systems: Current status and future directions. *Molecules* **26**, 5905 (2021).
2. Hu, Y. et al. Bioaccessibility and bioavailability of phytochemicals: Influencing factors, improvements, and evaluations. *Food Hydrocoll.* **135**, 108165. https://doi.org/10.1016/J.FOODHYD.2022.108165 (2023).
3. Wen, H., Jung, H. & Li, X. Drug delivery approaches in addressing clinical pharmacology-related issues: Opportunities and challenges. *AAPS J.* **17**, 1327 (2015).
4. Li, P. H., Wang, C. W. C. C. R., Lu, W. C., Song, T. Y. & Wang, C. W. C. C. R. Antioxidant, anti-inflammatory activities, and neuroprotective behaviors of *Phyllanthus emblica L.* fruit extracts. *Agric.* **12**, 588 (2022).
5. Halim, B. et al. Determination of phytochemical constituent, antioxidant activity, total phenol and total flavonoid of extract ethanol *Phyllanthus emblica* fruit. *Pharmacogn. J.* **14**, 63–67. https://doi.org/10.5530/pj.2022.14.9 (2022).
6. Mahata, S. et al. Anticancer activity of *Phyllanthus emblica L* inn. (Indian gooseberry): Inhibition of transcription factor AP-1 and HPV gene expression in cervical cancer cells. *Nutr. Cancer* **65**, 88–97. https://doi.org/10.1080/01635581.2013.785008 (2013).
7. Zhao, T., Sun, Q., Marques, M. & Witcher, M. Anticancer properties of *Phyllanthus emblica* (Indian gooseberry). *Oxid. Med. Cell. Longev.* **2015**, 950890 (2015).
8. Gouda, B. et al. Extraction, Phytochemical profile, and neuroprotective activity of Phyllanthus emblica fruit extract against sodium valproate-induced postnatal autism in BALB/c mice. *Heliyon* **10**. https://doi.org/10.1016/j.heliyon.2024.e34992 (2024).
9. Sai Ram, M. et al. Cyto-protective and immunomodulating properties of Amla (Emblica officinalis) on lymphocytes: an in-vitro study. *J. Ethnopharmacol.* **81**, 5–10. https://doi.org/10.1016/S0378-8741(01)00421-4 (2002).
10. Arjin, C. et al. In vitro screening antiviral activity of Thai medicinal plants against porcine reproductive and respiratory syndrome virus. *BMC Vet. Res.* **16**, 1–9. https://doi.org/10.1186/S12917-020-02320-8/TABLES/1 (2020).
11. Nawaz, H. et al. Optimization of Phyllanthus emblica L. leaf extract-assisted clearance of hyperbilirubinemia in White New Zealand albino rabbits. *All Life* **15**, 54–63. https://doi.org/10.1080/26895293.2021.2022006 (2022).
12. Quranayati, Q. et al. Effect of Phyllanthus emblicaL. stem bark extract on diabetic nephropathy and hyperlipidemia in rats. *J. Pharm. Pharmacogn. Res.* **11**, 308–314. https://doi.org/10.56499/JPPRES23.1595_11.2.308 (2023).
13. Wu, M. et al. The Composition and anti-aging activities of polyphenol extract from *Phyllanthus emblica L. Fruit. Nutr.* **14**, 857 (2022).
14. Yin, K. et al. Hepatoprotective effect and potential mechanism of aqueous extract from *Phyllanthus emblica* on carbon-tetrachloride-induced liver fibrosis in rats. *Evid. Based Complement. Altern. Med.* **2021**, 5345821 (2021).
15. Purena, R., Seth, R. & Bhatt, R. Protective role of *Emblica officinalis* hydro-ethanolic leaf extract in cisplatin induced nephrotoxicity in Rats. *Toxicol. Rep.* **5**, 270–277 (2018).
16. Srinivasan, P., Vijayakumar, S., Kothandaraman, S. & Palani, M. Anti-diabetic activity of quercetin extracted from *Phyllanthus emblica L.* fruit: In silico and in vivo approaches. *J. Pharm. Anal.* **8**, 109–118 (2018).
17. Muhacir-Güzel, N., Türkyilmaz, M., Yemiş, O., Tağı, Ş & Özkan, M. Changes in hydrolysable and condensed tannins of pomegranate (*Punica granatum L.*, cv. Hicaznar) juices from sacs and whole fruits during production and their relation with antioxidant activity. *LWT Food Sci. Technol.* **59**, 933–940 (2014).
18. Smeriglio, A., Barreca, D., Bellocco, E. & Trombetta, D. Proanthocyanidins and hydrolysable tannins: Occurrence, dietary intake and pharmacological effects. *Br. J. Pharmacol.* **174**, 1244–1262 (2017).
19. Yang, B. & Liu, P. Composition and biological activities of hydrolyzable tannins of fruits of *Phyllanthus emblica. J. Agric. Food Chem.* **62**, 529–541 (2014).
20. Batiha, G. E. S. et al. *Syzygium aromaticum L* (Myrtaceae): Traditional uses, bioactive chemical constituents. *Pharmacol. Toxicol. Act. Biomol.* **10**, 202 (2020).
21. Maggini, V. et al. Antimicrobial activity of *Syzygium aromaticum* essential oil in human health treatment. *Mol.* **29**, 999 (2024).
22. Kiki, M. J. In vitro antiviral potential, antioxidant, and chemical composition of clove (*Syzygium aromaticum)* essential oil. *Mol.* **28**, 2421 (2023).
23. Selles, S. M. A., Kouidri, M., Belhamiti, B. T. & Ait Amrane, A. Chemical composition, in-vitro antibacterial and antioxidant activities of *Syzygium aromaticum* essential oil. *J. Food Meas. Charact.* **14**, 2352–2358 (2020).
24. Permatasari, H. K., Effendi, A. B., Qhabibi, F. R., Fawwaz, F. & Dominique, A. Eugenol isolated from *Syzygium aromaticum* inhibits HeLa cancer cell migration by altering epithelial-mesenchymal transition protein regulators. *J. Appl. Pharm. Sci.* **11**, 049–053 (2021).
25. Huang, W. C. et al. Eugenol suppresses platelet activation and mitigates pulmonary thromboembolism in humans and murine models. *Int. J. Mol. Sci.* **25**, 2098 (2024).
26. Batiha, G. E. S. et al. Inhibitory effects of *Syzygium aromaticum* and *Camellia sinensis* methanolic extracts on the growth of Babesia and Theileria parasites. *Ticks Tick. Borne. Dis.* **10**, 949–958 (2019).
27. Haro-González, J. N., Castillo-Herrera, G. A., Martínez-Velázquez, M. & Espinosa-Andrews, H. Clove essential oil (*Syzygium aromaticum L* Myrtaceae): Extraction, chemical composition, food applications, and essential bioactivity for human health. *Mol.* **26**, 6387 (2021).
28. Özbek, Z. A. & Ergönül, P. G. Clove (*Syzygium aromaticum*) and eugenol toxicity. *Clove Syzygium Aromat. Chem. Funct. Appl.* https://doi.org/10.1016/B978-0-323-85177-0.00029-X (2022).
29. Pavan, B. et al. Pharmacokinetic and permeation studies in rat brain of natural compounds led to investigate eugenol as direct activator of dopamine release in PC12 cells. *Int. J. Mol. Sci.* **24**, 1800 (2023).
30. Jadhav, S., Gaikwad, S., Nimse, M. & Rajbhoj, A. Copper oxide nanoparticles: Synthesis, characterization and their antibacterial activity. *J. Clust. Sci.* **22**, 121–129 (2011).
31. Hosseini-Koupaei, M. et al. Catalytic activity, structure and stability of proteinase K in the presence of biosynthesized CuO nanoparticles. *Int. J. Biol. Macromol.* **122**, 732–744 (2019).
32. Zughaibi, T. A. et al. Evaluation of anticancer potential of biogenic copper oxide nanoparticles (CuO NPs) against breast cancer. *J. Nanomater.* **2022**, 5326355 (2022).
33. Etefagh, R., Azhir, E. & Shahtahmasebi, N. Synthesis of CuO nanoparticles and fabrication of nanostructural layer biosensors for detecting Aspergillus niger fungi. *Sci. Iran.* **20**, 1055–1058 (2013).
34. Naz, S., Gul, A., Zia, M. & Javed, R. Synthesis, biomedical applications, and toxicity of CuO nanoparticles. *Appl. Microbiol. Biotechnol.* **107**(4), 1039–1061 (2023).
35. Balcucho, J., Narváez, D. M. & Castro-Mayorga, J. L. Antimicrobial and biocompatible polycaprolactone and copper oxide nanoparticle wound dressings against methicillin-resistant *Staphylococcus aureus*. *Nanomaterials* **10**, 1692 (2020).

36. Ibne Shoukani, H. et al. Green synthesis of polyethylene glycol coated, ciprofloxacin loaded CuO nanoparticles and its antibacterial activity against *Staphylococcus aureus*. *Sci. Rep.* **141**(14), 1–18 (2024).
37. Assadian, E. et al. Toxicity of copper oxide (CuO) nanoparticles on human blood lymphocytes. *Biol. Trace Elem. Res.* **184**, 350–357 (2018).
38. Viswanadha, L. S., Arcot, Y., Lin, Y. T. & Akbulut, M. E. S. A comparative investigation of release kinetics of paclitaxel from natural protein and macromolecular nanocarriers in nanoscale drug delivery systems. *JCIS Open* **15**, 100120 (2024).
39. Thapa Magar, K., Boafo, G. F., Li, X., Chen, Z. & He, W. Liposome-based delivery of biological drugs. *Chinese Chem. Lett.* **33**, 587–596 (2022).
40. Dhahir, R. K., Al-Nima, A. M. & Al-Bazzaz, F. Y. Nanoemulsions as ophthalmic drug delivery systems. *Turkish J. Pharm. Sci.* **18**, 652 (2021).
41. Kianfar, E. Magnetic nanoparticles in targeted drug delivery: A review. *J. Supercond. Nov. Magn.* **347**(34), 1709–1735 (2021).
42. Thang, N. H., Chien, T. B. & Cuong, D. X. Polymer-based hydrogels applied in drug delivery: An overview. *Gels* **9**, 523 (2023).
43. Baishya, R., Hati Boruah, J. L., Bordoloi, M. J., Kumar, D. & Kalita, P. Novel drug delivery system in phytochemicals: Modern era of ancient science. *Herb. Med. India Indig. Knowl. Pract. Innov. its Value* https://doi.org/10.1007/978-981-13-7248-3_12 (2020).
44. Gaur, M., Maurya, S., Akhtar, M. S. & Yadav, A. B. Synthesis and evaluation of BSA-loaded PLGA-chitosan composite nanoparticles for the protein-based drug delivery system. *ACS Omega* **8**, 18751–18759 (2023).
45. Yadav, P. et al. Biocompatible drug delivery system based on a mof platform for a sustained and controlled release of the poorly soluble drug norfloxacin. *ACS Omega* **8**, 28367–28375 (2023).
46. Zhang, Y. et al. Hyaluronic acid modified oral drug delivery system with mucoadhesiveness and macrophage-targeting for colitis treatment. *Carbohydr. Polym.* **313**, 120884 (2023).
47. Mohammadi, R., Saboury, A., Javanbakht, S., Foroutan, R. & Shaabani, A. Carboxymethylcellulose/polyacrylic acid/starch-modified Fe3O4 interpenetrating magnetic nanocomposite hydrogel beads as pH-sensitive carrier for oral anticancer drug delivery system. *Eur. Polym. J.* **153**, 110500 (2021).
48. Thambiliyagodage, C. et al. Recent advances in chitosan-based applications—A review. *Materials* https://doi.org/10.3390/ma16052073 (2023).
49. Aranaz, I. et al. Chitosan: An overview of its properties and applications. *Polym.* **13**, 3256 (2021).
50. Adimoolam, M. G., Amreddy, N., Nalam, M. R. & Sunkara, M. V. A simple approach to design chitosan functionalized Fe3O4 nanoparticles for pH responsive delivery of doxorubicin for cancer therapy. *J. Magn. Magn. Mater.* **448**, 199–207 (2018).
51. Ni, S. et al. GABAB receptor ligand-directed trimethyl chitosan/tripolyphosphate nanoparticles and their pMDI formulation for survivin siRNA pulmonary delivery. *Carbohydr. Polym.* **179**, 135–144 (2018).
52. Nair, S. S. Chitosan-based transdermal drug delivery systems to overcome skin barrier functions. *J. Drug Deliv. Ther.* **9**, 266–270 (2019).
53. Hongfeng, Z., El-Kott, A., Ezzat Ahmed, A. & Khames, A. Synthesis of chitosan-stabilized copper nanoparticles (CS–Cu NPs): Its catalytic activity for C–N and C–O cross-coupling reactions and treatment of bladder cancer. *Arab. J. Chem.* **14**, 103259 (2021).
54. Javed, R. et al. Chitosan capping of CuO nanoparticles: Facile chemical preparation, biological analysis, and applications in dentistry. *Int. J. Biol. Macromol.* **167**, 1452–1467 (2021).
55. Tran, C. D., Makuvaza, J., Munson, E. & Bennett, B. Biocompatible copper oxide nanoparticle composites from cellulose and chitosan: Facile synthesis, unique structure, and antimicrobial activity. *ACS Appl. Mater. Interfaces* **9**, 42503–42515 (2017).
56. Sarfraz, M. H. et al. Comparative analysis of phyto-fabricated chitosan, copper oxide, and chitosan-based CuO nanoparticles: antibacterial potential against *Acinetobacter baumannii* isolates and anticancer activity against HepG2 cell lines. *Front. Microbiol.* **14**, 1188743 (2023).
57. Anitha, A. et al. Curcumin-loaded N, O–carboxymethyl chitosan nanoparticles for cancer drug delivery. *J. Biomater. Sci. Polym. Ed.* **23**, 1381–1400 (2012).
58. Zhang, J., Tang, Q., Xu, X. & Li, N. Development and evaluation of a novel phytosome-loaded chitosan microsphere system for curcumin delivery. *Int. J. Pharm.* **448**, 168–174 (2013).
59. Arulmozhi, V., Pandian, K. & Mirunalini, S. Ellagic acid encapsulated chitosan nanoparticles for drug delivery system in human oral cancer cell line (KB). *Colloids Surf. B Biointerfaces* **110**, 313–320 (2013).
60. Zhai, G. & GuoLiu., T. Preparation and evaluation of quercetin-loaded lecithin-chitosan nanoparticles for topical delivery. *Int. J. Nanomedicine.* https://doi.org/10.2147/IJN.S22411 (2021).
61. Nallamuthu, I., Devi, A. & Khanum, F. Chlorogenic acid loaded chitosan nanoparticles with sustained release property, retained antioxidant activity and enhanced bioavailability. *Asian J. Pharm. Sci.* **10**, 203–211 (2015).
62. El-Houssiny, A. S., Kamel, N. A., Soliman, A. A. F., El-Messieh, S. L. A. & Abd-El-Nour, K. N. Preparation and characterisation of gallic acid loaded carboxymethyl chitosan nanoparticles as drug delivery system for cancer treatment. *Adv. Nat. Sci. Nanosci. Nanotechnol.* **13**, 025002 (2022).
63. Devmurari, V. P. Antibacterial evaluation and phytochemical screening of *Symplocos Racemosa Roxb*. *Int. J. PharmTech. Res.* **2**, 1359–1363 (2010).
64. Siddiqui, M. Phytochemical analysis of some medicinal plants. *Liaquat. Med. Res. J.* **3**, 1–5 (2021).
65. Thambiliyagodage, C. et al. Persulfate assisted photocatalytic and antibacterial activity of TiO2–CuO coupled with graphene oxide and reduced graphene oxide. *Sci. Rep.* **14**, 12505 (2024).
66. Li, W. et al. HPLC fingerprint analysis of *Phyllanthus emblica* ethanol extract and their antioxidant and anti-inflammatory properties. *J. Ethnopharmacol.* **254**, 112740 (2020).
67. Yang, B., Kortesniemi, M., Liu, P., Karonen, M. & Salminen, J. P. Analysis of hydrolyzable tannins and other phenolic compounds in emblic leafflower (*Phyllanthus emblica L.)* fruits by high performance liquid chromatography-electrospray ionization mass spectrometry. *J. Agric. Food Chem.* **60**, 8672–8683 (2012).
68. Ma, Q. G. et al. *Phyllanthus emblica Linn*: A comprehensive review of botany, traditional uses, phytonutrients, health benefits, quality markers, and applications. *Food Chem.* **446**, 138891 (2024).
69. Liu, X. et al. Immunomodulatory and anticancer activities of phenolics from emblica fruit (*Phyllanthus emblica L.*). *Food Chem.* **131**, 685–690 (2012).
70. Saini, R., Kumar, V., Patel, C. N., Sourirajan, A. & Dev, K. Synergistic antibacterial activity of *Phyllanthus emblica* fruits and its phytocompounds with ampicillin: A computational and experimental study. *Naunyn. Schmiedebergs. Arch. Pharmacol.* **397**, 857–871 (2024).
71. Rubió, L., Motilva, M. J. & Romero, M. P. Recent advances in biologically active compounds in herbs and spices: A review of the most effective antioxidant and anti-inflammatory active principles. *Crit. Rev. Food Sci. Nutr.* **53**, 943–953 (2013).
72. Shariati, A. et al. Inhibitory effect of natural compounds on quorum sensing system in *Pseudomonas aeruginosa*: A helpful promise for managing biofilm community. *Front. Pharmacol.* **15**, 1350391 (2024).
73. Abdul Aziz, A. H. et al. Unlocking the full potential of clove (*Syzygium aromaticum)* spice: An overview of extraction techniques, bioactivity, and future opportunities in the food and beverage industry. *Process.* **11**, 2453 (2023).
74. Gulcin, I. Antioxidants and antioxidant methods: An updated overview. *Arch. Toxicol.* **943**(94), 651–715 (2020).
75. Saini, R. et al. Traditional uses, bioactive composition, pharmacology, and toxicology of *Phyllanthus emblica* fruits: A comprehensive review. *J. Ethnopharmacol.* **282**, 114570 (2022).
76. Kumar, G., Madka, V., Pathuri, G., Ganta, V. & Rao, C. V. Molecular mechanisms of cancer prevention by gooseberry *(Phyllanthus emblica)*. *Nutr. Cancer* **74**, 2291–2302 (2022).

77. Yi, F. et al. Chitosan/zein-based sustained-release composite films: Fabrication, physicochemical properties and release kinetics of tea polyphenols from polymer matrix. *Int. J. Biol. Macromol.* **269**, 131970 (2024).
78. Thanyacharoen, T., Chuysinuan, P., Techasakul, S., Nooeaid, P. & Ummartyotin, S. Development of a gallic acid-loaded chitosan and polyvinyl alcohol hydrogel composite: Release characteristics and antioxidant activity. *Int. J. Biol. Macromol.* **107**, 363–370 (2018).
79. Ozdal, T., Capanoglu, E. & Altay, F. A review on protein–phenolic interactions and associated changes. *Food Res. Int.* **51**, 954–970 (2013).
80. Amessis-Ouchemoukh, N., Madani, K., Falé, P. L. V., Serralheiro, M. L. & Araújo, M. E. M. Antioxidant capacity and phenolic contents of some mediterranean medicinal plants and their potential role in the inhibition of cyclooxygenase-1 and acetylcholinesterase activities. *Ind. Crops Prod.* **53**, 6–15 (2014).
81. Ambati, G. G. & Jachak, S. M. Natural product inhibitors of cyclooxygenase (COX) enzyme: A review on current status and future perspectives. *Curr. Med. Chem.* **28**, 1877–1905 (2020).
82. Pientaweeratch, S., Panapisal, V. & Tansirikongkol, A. Antioxidant, anti-collagenase and anti-elastase activities of *Phyllanthus emblica*, *Manilkara zapota* and silymarin: An in vitro comparative study for anti-aging applications. *Pharm. Biol.* **54**, 1865–1872 (2016).
83. Orabi, M. A. A. et al. Nutritional, antioxidant, antimicrobial, and anticholinesterase properties of *Phyllanthus emblica*: A study supported by spectroscopic and computational investigations. *Metabolites* **13**, 1013 (2023).
84. Mohyuddin, S. G. et al. Effect of chitosan on blood profile, inflammatory cytokines by activating TLR4/NF-κB signaling pathway in intestine of heat stressed mice. *Sci. Rep.* **111**(11), 1–13 (2021).
85. Krishnamurthy, N. B. et al. HR-LCMS assisted phytochemical screening of antioxidant, antibacterial activity of *Priva cordifolia (L.f)* Druce plant and molecular docking approach. *Results Chem.* **5**, 100794 (2023).
86. Sousa, A. D. et al. Ultrasound-assisted and pressurized liquid extraction of phenolic compounds from *Phyllanthus amarus* and its composition evaluation by UPLC-QTOF. *Ind. Crops Prod.* **79**, 91–103 (2016).
87. Faqer, O. E. et al. Phytochemical characterization and immunomodulatory effects of aqueous, ethanolic extracts and essential oil of *Syzygium aromaticum L.* on human neutrophils. *Sci. African* **18**, e01395 (2022).
88. Asghar, B. H. et al. Cross-linked quaternized chitosan nanoparticles for effective delivery and controllable release of *O. europaea* phenolic extract targeting cancer therapy. *J. Drug Deliv. Sci. Technol.* **83**, 104388 (2023).
89. Mary, T. R. N. & Jayavel, R. Fabrication of chitosan/cashew nut shell liquid/plant extracts-based bio-formulated nanosheets with embedded iron oxide nanoparticles as multi-functional barrier resist eco-packaging material. *Appl. Nanosci.* **12**, 1719–1730 (2022).
90. Rajaei, M. et al. Chitosan/agarose/graphene oxide nanohydrogel as drug delivery system of 5-fluorouracil in breast cancer therapy. *J. Drug Deliv. Sci. Technol.* **82**, 104307 (2023).
91. Lohiya, G. & Katti, D. S. Carboxylated chitosan-mediated improved efficacy of mesoporous silica nanoparticle-based targeted drug delivery system for breast cancer therapy. *Carbohydr. Polym.* **277**, 118822 (2022).
92. Ji, X. et al. Injectable immunomodulation-based porous chitosan microspheres/HPCH hydrogel composites as a controlled drug delivery system for osteochondral regeneration. *Biomaterials* **285**, 121530 (2022).
93. Rajabzadeh-Khosroshahi, M. et al. Chitosan/agarose/graphitic carbon nitride nanocomposite as an efficient pH-sensitive drug delivery system for anticancer curcumin releasing. *J. Drug Deliv. Sci. Technol.* **74**, 103443 (2022).
94. Homayouni Tabrizi, M. Fabrication of folic acid-conjugated chitosan-coated PLGA nanoparticles for targeted delivery of *Peganum harmala* smoke extract to breast cancer cells. *Nanotechnology* **33**, 495101 (2022).
95. Gomathi, M. et al. Novel drug delivery materials: Chitosan polymers conjugated with Spondias pinnata phytocompounds for enhanced anti-microbial and anti-cancer properties. *Polym. Adv. Technol.* **35**, e6561 (2024).
96. Wijayawardana, S., Thambiliyagodage, C. & Jayanetti, M. Kinetic study of in vitro release of curcumin from chitosan biopolymer and the evaluation of biological efficacy. *Arab. J. Chem.* **17**, 105896 (2024).
97. Katouzian, I. & Taheri, R. A. Preparation, characterization and release behavior of chitosan-coated nanoliposomes (chitosomes) containing olive leaf extract optimized by response surface methodology. *J. Food Sci. Technol.* **58**, 3430–3443 (2021).
98. Morsy, E. A., Hussien, A. M., Ibrahim, M. A., Farroh, K. Y. & Hassanen, E. I. Cytotoxicity and genotoxicity of copper oxide nanoparticles in chickens. *Biol. Trace Elem. Res.* **199**, 4731–4745 (2021).
99. Kaningini, A. G., Motlhalamme, T., More, G. K., Mohale, K. C. & Maaza, M. Antimicrobial, antioxidant, and cytotoxic properties of biosynthesized copper oxide nanoparticles (CuO-NPs) using Athrixia phylicoides DC. *Heliyon* **9**(4). https://doi.org/10.1016/j.heliyon.2023.e15265 (2023).
100. Liu, B., Poolman, B. & Boersma, A. J. Ionic strength sensing in living cells. *ACS Chem. Biol.* **12**, 2510–2514 (2017).
101. Kellum, J. A. Determinants of blood pH in health and disease. *Crit. Care* **4**, 6 (2000).
102. Kato, Y. et al. Acidic extracellular microenvironment and cancer. *Cancer Cell Int.* **13**, 89 (2013).
103. Stull, F., Hipp, H., Stockbridge, R. B. & Bardwell, J. C. A. In vivo chloride concentrations surge to proteotoxic levels during acid stress. *Nat. Chem. Biol.* **14**, 1051 (2018).
104. Akcay Ogur, F., Mamasoglu, S., Perry, S. L., Akin, F. A. & Kayitmazer, A. B. Interactions between hyaluronic acid and chitosan by isothermal titration calorimetry: The effect of ionic strength, pH, and polymer molecular weight. *J. Phys. Chem. B* https://doi.org/10.1021/ACS.JPCB.4C03930/SUPPL_FILE/JP4C03930_SI_001.PDF (2024).
105. Lee, J. H. & Yeo, Y. controlled drug release from pharmaceutical nanocarriers. *Chem. Eng. Sci.* **125**, 75 (2014).
106. Hassanpour, M. et al. Salicylic acid-loaded chitosan nanoparticles (SA/CTS NPs) for breast cancer targeting: Synthesis, characterization and controlled release kinetics. *J. Mol. Struct.* **1245**, 131040 (2021).
107. Jafari, H., Hassanpour, M., Rahmani, Z., Rezaie, J. & Akbari, A. Phenylalanine-encapsulated chitosan nanoparticles: Synthesis, characterization, controlled release kinetics and cytotoxicity evaluation. *J. Mol. Struct.* **1341**, 142627 (2025).
108. Nazari, M., Safaeijavan, R., Vaziri Yazdi, A. & Moniri, E. Investigation of the adsorption and release kinetics of the anticancer drug, methotrexate, from chitosan nanocapsules modified by caffeic acid and oleic acid. *Inorg. Chem. Commun.* **153**, 110769 (2023).
109. Kariminia, S., Shamsipur, A. & Shamsipur, M. Analytical characteristics and application of novel chitosan coated magnetic nanoparticles as an efficient drug delivery system for ciprofloxacin Enhanced drug release kinetics by low-frequency ultrasounds. *J. Pharm. Biomed. Anal.* **129**, 450–457 (2016).
110. Adlin Jino Nesalin, J. & Anton Smith, A. Preparation and evaluation of stavudine loaded chitosan nanoparticles. *J. Pharm. Res.* **6**, 268–274 (2014).
111. Saputra, O. A., Safitriono, W. N., Maharani, D. E. K., Febiana, A. & Wibowo, F. R. pH-controlled release feature of chitosan assembled silica nanoparticles containing nano-formulated curcumin over in vitro gastric and physiological condition. *Food Biosci.* **53**, 102793 (2023).
112. Ezike, T. C. et al. Advances in drug delivery systems, challenges and future directions. *Heliyon* **9**, e17488 (2023).
113. Fu, Y. & Kao, W. J. Drug release kinetics and transport mechanisms of non-degradable and degradable polymeric delivery systems. *Expert Opin. Drug Deliv.* **7**, 429 (2010).
114. Bayer, I. S. Controlled drug release from nanoengineered polysaccharides. *Pharmaceutics* **15**, 1364 (2023).
115. Unagolla, J. M. & Jayasuriya, A. C. Drug transport mechanisms and in vitro release kinetics of vancomycin encapsulated chitosan-alginate polyelectrolyte microparticles as a controlled drug delivery system. *Eur. J. Pharm. Sci.* **114**, 199–209 (2018).

116. Jadidi, A., Davoodian, F. & Salahinejad, E. Effect of poly lactic-co-glycolic acid encapsulation on drug delivery kinetics from vancomycin-impregnated Ca–Mg silicate scaffolds. *Prog. Org. Coat.* **149**, 105970 (2020).
117. Peppas, N. A. & Narasimhan, B. Mathematical models in drug delivery: How modeling has shaped the way we design new drug delivery systems. *J. Control Release* **190**, 75–81. https://doi.org/10.1016/j.jconrel.2014.06.041 (2014).
118. Paul, D. R. Elaborations on the Higuchi model for drug delivery. *Int. J. Pharm.* **418**, 13–17 (2011).
119. Askarizadeh, M., Esfandiari, N., Honarvar, B., Sajadian, S. A. & Azdarpour, A. Kinetic modeling to explain the release of medicine from drug delivery systems. *ChemBioEng Rev.* **10**, 1006–1049 (2023).
120. Molavi, F., Hamishehkar, H. & Nokhodchi, A. Impact of tablet shape on drug dissolution rate through immediate released tablets. *Adv. Pharm. Bull.* **10**, 656 (2020).
121. Wsoo, M. A. et al. Vitamin D3-loaded electrospun cellulose acetate/polycaprolactone nanofibers: Characterization, in-vitro drug release and cytotoxicity studies. *Int. J. Biol. Macromol.* **181**, 82–98 (2021).
122. Jiang, K., Zhou, X. & He, T. The synthesis of bacterial cellulose-chitosan zwitterionic hydrogels with pH responsiveness for drug release mechanism of the naproxen. *Int. J. Biol. Macromol.* **209**, 814–824 (2022).
123. Cheba, B. A. Chitosan: Properties, modifications and food nanobiotechnology. *Procedia Manuf.* **46**, 652–658 (2020).
124. Ke, C. L., Deng, F. S., Chuang, C. Y. & Lin, C. H. Antimicrobial actions and applications of chitosan. *Polym.* **13**, 904 (2021).
125. Amalraj, A., Haponiuk, J. T., Thomas, S. & Gopi, S. Preparation, characterization and antimicrobial activity of polyvinyl alcohol/gum arabic/chitosan composite films incorporated with black pepper essential oil and ginger essential oil. *Int. J. Biol. Macromol.* **151**, 366–375 (2020).
126. Garavand, F. et al. A comprehensive review on the nanocomposites loaded with chitosan nanoparticles for food packaging. *Crit. Rev. Food Sci. Nutr.* **62**, 1383–1416 (2022).
127. Mendis, A. et al. Fabrication of naturally derived chitosan and ilmenite sand-based TiO_2/Fe_2O_3/Fe-N-doped graphitic carbon composite for photocatalytic degradation of methylene blue under sunlight. *Molecules* **28**. https://doi.org/10.3390/molecules28073154 (2023).
128. Ul-Islam, M. et al. Chitosan-based nanostructured biomaterials: Synthesis, properties, and biomedical applications. *Adv. Ind. Eng. Polym. Res.* **7**, 79–99 (2024).
129. Alqahtani, F. et al. Antibacterial activity of chitosan nanoparticles against pathogenic N. gonorrhoea. *Int. J. Nanomedicine* 7877–7887 (2020).
130. Goy, R. C., De Britto, D. & Assis, O. B. G. A review of the antimicrobial activity of chitosan. *Polímeros* **19**, 241–247 (2009).
131. Ardean, C. et al. Factors influencing the antibacterial activity of chitosan and chitosan modified by functionalization. *Int. J. Mol. Sci.* https://doi.org/10.3390/ijms22147449 (2021).
132. Dulta, K. et al. Multifunctional CuO nanoparticles with enhanced photocatalytic dye degradation and antibacterial activity. *Sustain. Environ. Res.* **32**, 1–15 (2022).
133. Meghana, S., Kabra, P., Chakraborty, S. & Padmavathy, N. Understanding the pathway of antibacterial activity of copper oxide nanoparticles. *RSC Adv.* **5**, 12293–12299 (2015).
134. Dadi, R., Azouani, R., Traore, M., Mielcarek, C. & Kanaev, A. Antibacterial activity of ZnO and CuO nanoparticles against gram positive and gram negative strains. *Mater. Sci. Eng. C* **104**, 1–16 (2019).
135. Ren, G. et al. Characterisation of copper oxide nanoparticles for antimicrobial applications. *Int. J. Antimicrob. Agents* **33**, 587–590 (2009).
136. Suárez-Cerda, J. et al. A green synthesis of copper nanoparticles using native cyclodextrins as stabilizing agents. *J. Saudi Chem. Soc.* **21**, 341–348 (2017).
137. Tadjarodi, A. & Roshani, R. A green synthesis of copper oxide nanoparticles by mechanochemical method growing science. *Curr. Chem. Lett.* **3**, 215–220 (2014).
138. Yuan, P., Ding, X., Yang, Y. Y. & Xu, Q. H. Metal nanoparticles for diagnosis and therapy of bacterial infection. *Adv. Healthc. Mater.* **7**, 1701392 (2018).
139. Guan, G. et al. Antibacterial properties and mechanism of biopolymer–based films functionalized by CuO/ZnO nanoparticles against *Escherichia coli* and *Staphylococcus aureus*. *J. Hazard. Mater.* **402**, 123542 (2021).
140. Javed, R., Ahmed, M., Haq, I. U., Nisa, S. & Zia, M. PVP and PEG doped CuO nanoparticles are more biologically active: Antibacterial, antioxidant, antidiabetic and cytotoxic perspective. *Mater. Sci. Eng. C* **79**, 108–115 (2017).
141. Alipour, A., Javanshir, S. & Peymanfar, R. Preparation, characterization and antibacterial activity investigation of hydrocolloids based irish moss/ZnO/CuO bio-based nanocomposite films. *J. Clust. Sci.* **29**, 1329–1336 (2018).
142. Das, D., Nath, B. C., Phukon, P. & Dolui, S. K. Synthesis and evaluation of antioxidant and antibacterial behavior of CuO nanoparticles. *Colloids Surf. B Biointerfaces* **101**, 430–433 (2013).
143. Sonia, S. et al. Synthesis of hierarchical CuO nanostructures: Biocompatible antibacterial agents for gram-positive and gram-negative bacteria. *Curr. Appl. Phys.* **16**, 914–921 (2016).
144. Rodríguez-Barajas, N., de Jesús Martín-Camacho, U. & Pérez-Larios, A. Mechanisms of metallic nanomaterials to induce an antibacterial effect. *Curr. Top. Med. Chem.* **22**, 2506–2526 (2022).
145. Mirbagheri, V. S. et al. Toward understanding the antibacterial mechanism of chitosan: Experimental approach and in silico analysis. *Food Hydrocoll.* **147**, 109382 (2024).
146. Tsai, G. J. & Su, W. H. Antibacterial activity of shrimp chitosan against *Escherichia coli*. *J. Food Prot.* **62**, 239–243 (1999).
147. Sudarshan, N. R., Hoover, D. G. & Knorr, D. Antibacterial action of chitosan. *Food Biotechnol.* **6**, 257–272 (1992).
148. Raafat, D., Von Bargen, K., Haas, A. & Sahl, H. G. Insights into the mode of action of chitosan as an antibacterial compound. *Appl. Environ. Microbiol.* **74**, 3764–3773 (2008).
149. Kamat, S. & Kumari, M. Emergence of microbial resistance against nanoparticles: Mechanisms and strategies. *Front. Microbiol.* **14**, 1102615 (2023).
150. Bahrami, M. et al. How nanomaterials act against bacterial structures? A narrative review by focusing on molecular mechanism of the nanoparticles. *Microb. Pathog.* **196**, 107002 (2024).
151. Sun, R. et al. Overcoming nanosilver resistance: Resensitizing bacteria and targeting evolutionary mechanisms. *ACS Nano* **19**, 1702–1712 (2024).
152. Rajivgandhi, G., Maruthupandy, M. & Quero, F. Investigation of chitosan/metal and metal oxide nanocomposites as a new strategy for enhanced anti-biofilm efficacy with reduced toxicity. *Biol. Med. Phys. Ser.* https://doi.org/10.1007/978-981-19-9646-7_15 (2023).
153. Devliya, B., Patel, B., Chauhan, S. J. & Patel, H. D. A comprehensive review of nanomaterials as potential weapons against multidrug-resistant staphylococcus aureus. *Pharm. Nanotechnol.* **12**. https://doi.org/10.2174/0122117385314186240522100239 (2024).
154. Gauba, A. & Rahman, K. M. Evaluation of antibiotic resistance mechanisms in gram-negative bacteria. *Antibiotics* **12**, 1590 (2023).
155. Leus, I. V. et al. Functional diversity of gram-negative permeability barriers reflected in antibacterial activities and intracellular accumulation of antibiotics. *Antimicrob. Agents Chemother.* **67**, e01377 (2023).
156. Balan, G., Sofronie, O., Rusu, I. F., Tapu, L. & Burduniuc, O. Antimicrobial resistance mechanisms characteristic of clinically important gram-negative baccili. *Akad Rev Știință Inovare Cult și Artă*. https://doi.org/10.52673/18570461.22.4-67.04 (2023).
157. Kherroubi, L., Bacon, J. & Rahman, K. M. Navigating fluoroquinolone resistance in gram-negative bacteria: A comprehensive evaluation. *JAC-antimicrob. Resist.* **6**, 127 (2024).

158. Ferreira, S. R. S. et al. Colloidal copper oxide nanoparticles leading to a biphasic dose-response in growth inhibition of *Staphylococcus aureus*. *Future Microbiol.* **18**, 471–479 (2023).
159. Asamoah, R. B. et al. Synthesis and characterization of zinc and copper oxide nanoparticles and their antibacteria activity. *Results Mater.* **7**, 100099 (2020).
160. Sriyutha Murthy, P. et al. Antibiofilm activity of nano sized CuO. *Proc. Int. Conf. Nanosci. Eng. Technol. ICONSET* **2011**, 580–583. https://doi.org/10.1109/ICONSET.2011.6168037 (2011).
161. Maheo, A. R. Biosynthesis and characterization of *Eupatorium adenophorum* and chitosan mediated Copper oxide nanoparticles and their antibacterial activity. *Results Surf. Interfaces* **6**, 100048 (2022).
162. Umoren, P. S., Kavaz, D., Nzila, A., Sankaran, S. S. & Umoren, S. A. Biogenic synthesis and characterization of chitosan-CuO nanocomposite and evaluation of antibacterial activity against gram-positive and -negative bacteria. *Polymers (Basel).* **14**, 1832–1832 (2022).
163. Vieira, B. B., de Carvalho, E. A., da Rocha Bispo, A. S., Ferreira, M. A. & Evangelista-Barreto, N. S. Efficiency of chitosan synergism with clove essential oil in the coating of intentionally contaminated Tambaqui fillets. *Semin. Agrar.* **41**, 2793–2802. https://doi.org/10.5433/1679-0359.2020V41N6P2793 (2020).
164. Bai, J. et al. Antibacterial activity and mechanism of clove essential oil against foodborne pathogens. *LWT* **173**, 114249 (2023).
165. Ode, I. et al. The antibacterial activity of clove *Syzygium aromaticum* extract and its effects on the survival rate of hybrid grouper *Epinephelus fuscoguttatus* ♀ × *E. lanceolatus* ♂ infected with *Vibrio alginolyticus*. *J. Akuakultur Indones.* **22**, 1–11 (2023).
166. Marouf, R., Ermolaev, A. V., Podoprigora, I. V., Senyagin, A. N. & Mbarga, M. J. A. Antibacterial activity of clove *Syzygium aromaticum L.* and synergism with antibiotics against multidrug-resistant uropathogenic *E. coli*. *Rudn J. Med.* **27**, 379–390 (2023).
167. Sarojamma, V., Siddhartha, E. & Vadde, R. Antibacterial effect of indian gooseberry *(Phyllanthus emblica L.)* extract against ESBL producing multi-drug resistant bacteria. *J. Biomed. Res. Environ. Sci.* **5**, 227–232 (2024).
168. Devi, R., Potireddy, S., Rukmini, K., Prakasam, P. G. & Devamma, M. N. Phytochemical analysis and in vitro synergistic antibacterial effect of methanolic extracts of phyllanthus fruits against human pathogens. *Indian J. Pharm. Sci.* **86**. https://doi.org/10.36468/PHARMACEUTICAL-SCIENCES.1276 (2024).
169. Mariam Ali Kki Mohamed Ali, et al. Exploring the antimicrobial potential of *Phyllanthus emblica L.* (Amla) using molecular docking studies against shrimp pathogens. *J Adv Zool.* **44**, 447–456 (2023).
170. Jikah, A. N. & Edo, G. I. Mechanisms of action by sulphur compounds in *Allium sativum*. A review. *Pharmacol. Res. Mod. Chinese Med.* **9**, 100323 (2023).
171. Indira, M., Bhuvaneshwari, G., Premkumar, L. & Neelusree, P. Antibacterial activity of the allium sativum crude extract against methicillin-resistant *Staphylococcus aureus*. *J. Pure Appl. Microbiol.* **18**, 1297–1304 (2024).
172. Jayanetti, M. et al. In vitro influence of PEG functionalized ZnO–CuO nanocomposites on bacterial growth. *Sci. Rep.* **14**, 1–21 (2024).
173. Mogana, R., Adhikari, A., Tzar, M. N., Ramliza, R. & Wiart, C. Antibacterial activities of the extracts, fractions and isolated compounds from *Canarium patentinervium* miq. Against bacterial clinical isolates. *BMC Complement. Med. Ther.* **20**, 1–11 (2020).
174. Gonzalez, N. et al. Influence of the MBC/MIC ratio on the antibacterial activity of vancomycin versus linezolid against methicillin-resistant *Staphylococcus aureus* isolates in a pharmacodynamic model simulating serum and soft tissue interstitial fluid concentrations reported. *J. Antimicrob. Chemother.* **68**, 2291–2295 (2013).
175. Meylan, P. R., Francioli, P. & Glauser, M. P. Discrepancies between MBC and actual killing of viridans group streptococci by cell-wall-active antibiotics. *Antimicrob. Agents Chemother.* **29**, 418–423 (1986).
176. Abdallah, E. M. et al. In vitro influence of ZnO, CrZnO, RuZnO, and BaZnO nanomaterials on bacterial growth. *Molecules* **27**, 8309. https://doi.org/10.3390/MOLECULES27238309 (2022).
177. Swinnen, I. A. M., Bernaerts, K., Dens, E. J. J., Geeraerd, A. H. & Van Impe, J. F. Predictive modelling of the microbial lag phase: A review. *Int. J. Food Microbiol.* **94**, 137–159 (2004).
178. Wang, L., Fan, D., Chen, W. & Terentjev, E. M. Bacterial growth, detachment and cell size control on polyethylene terephthalate surfaces. *Sci. Rep.* **5**, 1–11 (2015).
179. Hazard. Saheed, I. O., Oh, W. Da & Suah, F. B. M. Chitosan modifications for adsorption of pollutants – A review. *J. Hazard. Mater.* **408**. https://doi.org/10.1016/j.jhazmat.2020.124889 (2021).
180. Cahyani, F., Farizaldi, R. I., Syafaati, L. M., Hartanli, A. L. & Aryandhita, A. P. P. Anti-microbial efficacy of garlic (*Allium Sativum L.*) extract as a root canal irrigant in endodontic treatment.. *Conserv. Dent. J Collect. J. Artic. Dent. Fac. Airlangga Univ.* **13**, 91–95 (2023).
181. Crini, G. Historical review on chitin and chitosan biopolymers. *Environ. Chem. Lett.* **17**, 1623–1643 (2019).
182. Naveen, K. V., Saravanakumar, K., Sathiyaseelan, A. & Wang, M. H. Preparation, characterization, and synergistic antibacterial activity of mycosynthesized, PEGylated CuO nanoparticles combined tetracycline hydrochloride. *J. Drug Deliv. Sci. Technol.* **76**, 1–2 (2022).
183. Chien, A. C., Hill, N. S. & Levin, P. A. Cell size control in bacteria. *Curr. Biol.* **22**, R340–R349 (2012).

Acknowledgements

The authors acknowledge the Sri Lanka Institute of Nanotechnology, the University of Sri Jayewardenepura and R&D Centre, Link Natural Products (Pvt) Ltd for providing instrument facilities.

Author contributions

G.E., S.W., M.J., H.L., and A.M. performed the experiments. G.E., M.J. and C.J., conceptualized, G.E., S.W., M.J., H.L., and C.J. analyzed the data, G.E., S.W., M.J.,A.M. and C.J., wrote the main manuscript, G.E., S.W., M.J., H.L., prepared all the figures, C.J. obtained funds, All authors reviewed the manuscript.

Funding

This research was supported by the Accelerating Higher Education Expansion and Development (AHEAD) Operation of the Ministry of Higher Education, funded by the World Bank. The authors thank the Sri Lanka Institute of Information Technology for providing part of the funding for this project.

Declarations

Competing interests

The authors declare no competing interests.

Additional information

Supplementary Information The online version contains supplementary material available at https://doi.org/10.1038/s41598-025-19914-7.

Correspondence and requests for materials should be addressed to C.T.

Reprints and permissions information is available at www.nature.com/reprints.

Publisher's note Springer Nature remains neutral with regard to jurisdictional claims in published maps and institutional affiliations.